Journal of Thermal Analysis and Calorimetry (2019) 135:1047–1067
https://doi.org/10.1007/s10973-018-7380-y

Conjugate natural convection of nanofluids inside an enclosure filled by three layers of solid, porous medium and free nanofluid using Buongiorno's and local thermal non-equilibrium models

S. A. M. Mehryan[1] · Mohammad Ghalambaz[2] · Mohsen Izadi[3]

Received: 9 April 2018 / Accepted: 15 May 2018 / Published online: 6 June 2018

Abstract
The natural convective heat transfer of nanofluids was addressed inside a square enclosure filled by three different layers: solid, porous medium and free fluid. The behavior of the porous layer has been simulated using local thermal non-equilibrium model. The Buongiorno's model was utilized to evaluate the distribution of nanoparticles inside the enclosure that arose from the thermophoresis and Brownian motion. The governing equations were solved by the Galerkin finite element method in a non-uniform grid. The governing parameters are Rayleigh number $Ra = 10^3$–10^6, porosity $\varepsilon = 0.3$–0.9, Darcy number $Da = 10^{-5}$–10^{-2}, interface parameter $K_r = 0.1$–10, $H = 0.1$–1000; ratio of wall thermal conductivity to that of the nanofluid, $R_k = 0.1$–10, dimensionless length of the heater $B = 0.2$–0.8; dimensionless centre position height of the heater $Z = 0.3$–0.7 and Lewis number $Le = 10$–100. A considerable concentration gradient of nanoparticles was found inside the enclosure. In some studied cases, the non-dimensional volume fraction of nanoparticles is about 10% higher than the average volume fraction of nanoparticles at the region near the cold wall. The variability of Darcy and the Rayleigh numbers indicated significant effects on heat transfer rate and the concentration patterns of the nanoparticles and inward the cavity. The increase in *Le* and *Nr* amplifies and decreases the heat transfer rates through fluid and solid phases, respectively. In addition, it can be seen that the increment in heat transfer rates with Le increases as *Nr* increases.

Keywords Buongiorno's model · Local thermal non-equilibrium · Porous medium layer · Free fluid layer · Solid layer

List of symbols

Latin symbols

b	Length of the heater (m)
B	Dimensionless length of the heater
C	Nanoparticle volume fraction
C_0	Ambient nanoparticle volume fraction
d	Wall thickness (m)
D	Dimensionless wall thickness
Da	Darcy number
D_B	Brownian diffusion coefficient
D_T	Thermophoresis diffusion coefficient
g	Gravitational acceleration vector (m s^{-2})
h_{nfs}	Volumetric heat transfer coefficient between the nanofluid and solid porous matrix (W m^{-3} K^{-1})
H	Interface heat transfer coefficient parameter
k	Thermal conductivity (W m^{-1} K^{-1})
K	Permeability of the porous medium (m^2)
K_r	Nanofluid to solid porous matrix thermal conductivity ratio parameter
L	Square cavity size (m)
Le	Lewis number
n	Normal vector (m)
N	Dimensionless normal vector
Nb	Brownian motion parameter

✉ Mohammad Ghalambaz
m.ghalambaz@iaud.ac.ir

S. A. M. Mehryan
alal171366244@gmail.com

Mohsen Izadi
izadi.m@lu.ac.ir

[1] Young Researchers and Elite Club, Yasooj Branch, Islamic Azad University, Yasooj, Iran

[2] Department of Mechanical Engineering, Dezful Branch, Islamic Azad University, Dezful, Iran

[3] Mechanical Engineering Department, Faculty of Engineering, Lorestan University, Khorramabad, Iran

Nr	Buoyancy ratio parameter
Nt	Thermophoresis parameter
Nu	Local Nusselt number
$\overline{Nu}$	Average Nusselt number
p	Pressure (Pa)
P	Dimensionless pressure
Pr	Prandtl number
q_{i}	Total interfacial heat flux (W m^{-2})
Q_{w}	Dimensionless local heat transfer through the wall
$\overline{Q_{\mathrm{w}}}$	Dimensionless average heat transfer through the wall
Ra	Rayleigh number
R_{k}	Wall to nanofluid thermal conductivity ratio parameter
s	Porous layer thickness (m)
S	Dimensionless porous layer thickness
Sh	Local Sherwood number
T	Temperature (K)
u, v	Velocity components along x, y directions, respectively (m s^{-1})
U, V	Dimensionless velocity components along x, y directions, respectively
x, y	Cartesian coordinates (m)
X, Y	Dimensionless Cartesian coordinates
z	Center position height of the heater (m)
Z	Dimensionless center position height of the heater

Greek symbols

α	Effective thermal diffusivity (m^2 s^{-1})
β	Thermal expansion coefficient of the fluid (K^{-1})
Δ	Difference value
ε	Porosity of the porous medium
θ	Dimensionless temperature
μ	Dynamic viscosity (kg m^{-1} s^{-1})
ν	Kinematic viscosity (m^2 s^{-1})
ρ	Density (kg m^{-3})
(ρc)	Effective heat capacity (J K^{-1} m^{-3})
τ	Parameter defined by $\tau = (\rho c)_{\mathrm{p}}/(\rho c)_{\mathrm{nf}}$
ϕ	Relative nanoparticle volume fraction
Ψ	Dimensionless stream function

Subscripts

0	Ambient property
c	Cold
eff	Effective
h	Hot
max	Maximum
nf	Nanofluid
p	Nanoparticle
s	Solid porous matrix
w	Wall

Introduction

Natural convection heat transfer arises from a change in the density of a working fluid, where there is no need for any external power or moving parts to induce a flow. Hence, the natural convection mechanism is simple and safe. In natural convection, the fluid motion is smooth and slow. Thus, there are very low noise levels in heat transfer devices manufactured based on such mechanism. Therefore, this heat transfer procedure inside a cavity has been the subject of many recent studies due to its important advantages. However, the main disadvantage of the natural convection is the complexity of the design and also its low capacity of heat transfer. Therefore, further investigations on the enhancement of the heat transfer via free convection mechanism are still demanded. Studies and applications of the natural convection can be seen in [1–4].

One method to improve the heat transfer rate is utilization of extended surfaces. In recent years, some researchers have applied very thermal conductive metals such as aluminum and copper to develop a porous medium structure, metal foam, with both high porosity and effective surface area [5–9]. In general, two main approaches exist for modeling heat transfer through porous media: the local thermal equilibrium (LTE) and the local thermal non-equilibrium (LTNE) approach [10]. For LTE approach, it is assumed that the pore solid walls and the captured fluid are at the same temperature, and hence, only one temperature represents the temperature of both domains [11]. However, when the thermal interplay between the pore walls and connected fluid is low or when the thermal conductivity of solid matrix is far higher than the thermal conductivity of the fluid, the temperature of the solid matrix may significantly differ from that of the fluid captured the pores. In such cases, two different domains should be defined to investigate thermal behavior of porous media. One domain represents the temperature of the solid matrix, and the other one denotes the temperature of the fluid captured the pores. Hence, LTNE models are also propounded as two-equation models [12, 13]. Considering natural convection heat transfer in metal foams, the LTNE models are demanded due to fact that the thermal conductivity of a metal foam is much higher than that of typical working fluids. Moreover, in natural convection flows, the fluid velocity is low and a low thermal interplay between the fluid and solid matrix can be also expected.

There are numerous researches in the literature, addressing the natural convection heat transfer in porous enclosures using LTE and LTNE models [14–16]. The books by Nield and Bejan [10] as well as Vafai [17] provide a thorough review of these pieces of research. There are only few studies that have considered the conjugate

conduction-natural convection heat transfer through porous media using LTNE model [18]. Indeed, by considering conjugate heat transfer using LTNE, there are difficulties in modeling and satisfying the temperature continuity and energy balance at the interface of different three layers located inside the cavity [19, 20].

Another way to enhance the heat transfer is using enhanced thermal conductivity of the working fluid. Experiments show that scattering a small volume fraction of nanoparticles in a conventional fluid can enhance the overall thermal conductivity of the resulted mixture [21–28]. A synthesized stable mixture of nanoparticles and a conventional thermal fluid is known as a nanofluid. The nanofluids also seem promising for enhancing convection heat transfer across a wide range of industrial applications [29].

According to one perspective, there are two models for the study of heat transfer of nanofluids. One is the homogeneous mixture model, known as the static model, for which a uniform mixture of nanoparticles and the base fluid is assumed. In the homogeneous mixture, model no relative movement between the nanoparticles and base fluid is allowed [30–33]. The other more advanced model, which can represent the behavior of the nanoparticles, is the mixture model, proposed by Buongiorno. Buongiorno's model considers a relative movement between the nanoparticles and the base fluid [34–37]. Buongiorno has concluded that the thermophoresis and Brownian forces, action on the nanoparticles in a nanofluid, are the important nanoscale mechanisms for nanofluids and can result in a significant concentration gradient of nanoparticles. The thermophoresis force usually carries the nanoparticles along a direction across from the temperature gradient. Conversely, the Brownian motion force typically homogenizes the nanoparticles inside the base fluid. Hence, a nanofluid which experiences a temperature gradient would experience a concentration gradient [38–42]. As a result, the concentration gradient of the heavy nanoparticles can affect the buoyancy forces and other aspects of flow and heat transfer in the nanofluids [43, 44].

Considering the homogeneous model of nanofluids, Alsabery et al. [45] have performed the conjugate conduction-natural convection heat transfer inside a trapezoidal enclosure. Alsabery et al. [45] reported that the average Nusselt number significantly increased with increasing nanoparticle volume fractions. This arises from higher thermal conductivity of the nanoparticles compared to base fluid. Alsabery et al. [46] have also studied the transient natural convection of nanofluids inside a trapezoidal cavity. Sheikholeslami and Ganji [47] also Sheikholeslami and Chamkha [48] have addressed the natural convection heat transfer of nanofluids in a collector enclosure with sine shape walls subjected to a magnetic field on. Bondareva et al. [49] have investigated the conjugate heat transfer of nanofluids inside a porous cavity. Considering the Buongiorno's model, Sheikholeslami and Chamkha [50] as well as Reddy and Chamkha [51] and Reddy et al. [52] have analyzed the force convective heat transfer of nanofluids over confined. There are also very recent studies that have analyzed the natural convection heat transfer of nanofluids inside a cavity using the Buongiorno's mathematic model such as [42, 53, 54]. As a summary, the convection heat transfer of nanofluids through porous media has been studied in recent researches of Kasaeian et al. [55] and Sheikholeslami [56, 57].

Systems that consist of multilayer media, a layer of solid shell wall, a layer of saturated porous medium and a free fluid layer are very common in industrial applications. For instance, an enclosure metal tank partially filled with grains is a common example of such a system, where the metal sheet of the tank shell is the solid layer, the grains are the porous medium layer, and the free space over the grains is the free layer. Although there are a wide range of industrial applications for such systems, there are only few studies, which have addressed the convective heat transfer in multilayer systems.

Considering a cavity partially saturated by a porous medium, the mixed convection of nanofluids in a partly layered porous enclosure with an internally revolving cylinder by Chamkha et al. [58] using the homogeneous model of nanofluids and assuming LTE model. Chamkha and Ismael [59] have addressed the natural convection heat transfer of nanofluids in a cavity partly saturated with a layer of porous medium filled by a nanofluid. The nanofluid was modeled as a homogeneous mixture, where the porous matrix and the nanofluid were considered to be in local thermal equilibrium. Hence, there are no concentration gradients of nanoparticles. In addition, no temperature difference between the fluid and the solid matrix is allowed. The natural convection of nanofluids inside a tilted trapezoid enclosure partly filled with a layer of porous medium has been examined by Alsabery et al. [60]. Further, in a very recent study [59], Ismael and Chamkha [61] have addressed the nanofluids' convection heat transfer in a square cavity. The top and bottom walls of the cavity were well insulated, and the right vertical side wall was at the isothermal temperature of T_h, while the left wall was at the isothermal cold temperature of T_c. There was a layer of solid over the hot wall, and then there was a layer of a porous medium over the solid layer, and finally there was a layer of free fluid between the cold wall and the porous layer. As with [59, 60], Ismael and Chamkha [61] also have utilized the homogeneous model of nanofluids using local thermal equilibrium (LTE) model.

Following the study of Ismael and Chamkha [61], in the present study, a non-homogeneous model of nanofluids,

Buongiorno's model, is adopted to capture the concentration gradients of nanoparticles. In addition, LTNE model is adopted to model the conjugate heat transfer inside the porous layer. The main physical contributions of the present study are (a) considering a concentration gradient for nanoparticles and (b) considering the temperature discrepancy between two elements of the porous medium layer. The aim of the study is to analyze the conjugate heat transfer of nanofluids inside a cavity filled by multilayers using LTNE and Buongiorno's model.

Definition of the problem and mathematical formulation

Figure 1 demonstrates a schema of the physical model for conjugate natural convection heat transfer in a multilayer cavity. The studied square domain with the length of L was divided into three parts of solid, porous medium and nanofluid, where the width of the solid and the porous medium are denoted by s and d, respectively. Here, s and d were adopted as $0.1L$ and $0.45L$, respectively. As pictured in Fig. 1, a flash heater with hot temperature T_h and length b was embedded on the left wall with the center position height of z. The other parts of the left wall along with the entire top and bottom walls were well insulated. The entire right wall was held at the isothermal cold temperature T_c.

The following physical points have been taken into consideration in modeling the conjugate heat transfer in the cavity. The condition of no-slip boundary remained true on the solid surfaces. The porous medium included a solid matrix, and the pores were filled with an incompressible nanofluid such that all the pores of the porous region were occupied by the nanofluid. The solid matrix was assumed as isotropic and homogenous. In addition, the nanofluid was assumed Newtonian and its flow in the pores was laminar. Due to very low size of nanoparticles, the nanoparticles and the base fluid were assumed to be at the same temperature. However, there was a temperature difference between the porous matrix and the nanofluid inside the pores, and hence, the local thermal non-equilibrium model was used to consider heat transport through the porous medium. In the cases such as the metal foams, in which the thermal conductivity of the porous matrix is much higher than the thermal conductivity of the fluid inside the pores, the temperature of the porous matrix can significantly differ from the temperature of the fluid inside the pores due to the heat transfer through the porous matrix. This temperature difference can be boosted in a situation in which the convective heat transfer coefficient between the fluid and porous matrix structures is low. Such a low convective heat transfer coefficient can be seen in natural convective heat transfer where the fluid velocities are low. Hence, in such cases the LTNE model is more accurate and has been adopted in the present study. Moreover, it was assumed that the solid nanoparticles were always stable and suspended in the base fluid, meaning that there was no sedimentation and accumulation of the nanoparticles. Apart from density, all the thermophysical characteristics of the nanofluid were regarded as constant. The impact of the buoyancy volume force was considered using Boussinesq approximation model. The gravity acceleration vector acted in the direction of the negative y, as revealed in Fig. 1. In this study, the non-homogenous dispersion of solid nanoparticles in the fluid was modeled using Buongiorno's model [34]. Buongiorno [34], using the scale analysis, has discussed several nanoscale forces which can affect the movement of nanoparticles in a nanofluid. Among these forces, the thermophoresis and Brownian motion forces found to be important. The thermophoresis force tends to move the nanoparticles from hot to the cold due to the difference in momentum of molecules in the hot and cold sides of a nanoparticle. In contrast, the Brownian motion tends to uniform the nanoparticles in the nanofluid. Since Buongiorno's model [34] includes the migration effect of nanofluids, this model has been adopted in the present study to simulate the concentration gradients of nanoparticles as well as flow and heat transfer in the cavity.

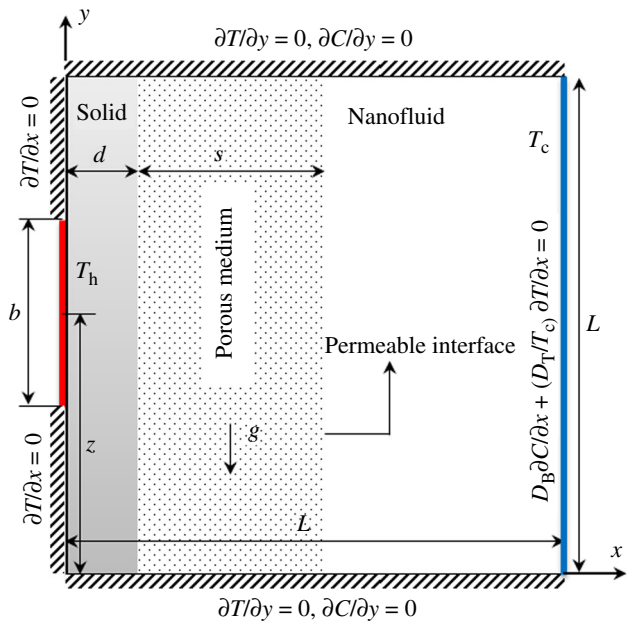

Fig. 1 Schematic view of the present problem

Considering the assumptions mentioned above, the set of governing equation for the nanofluid flow and heat transfer in the free layer were written as follows [10, 34, 62]:

$$\frac{\partial u}{\partial x}+\frac{\partial v}{\partial y}=0 \tag{1}$$

$$\rho_{\mathrm{nf}}\left(u\frac{\partial u}{\partial x}+v\frac{\partial u}{\partial y}\right)=-\frac{\partial p}{\partial x}+\mu_{\mathrm{nf}}\left(\frac{\partial^2 u}{\partial x^2}+\frac{\partial^2 u}{\partial y^2}\right) \tag{2}$$

$$\begin{aligned}\rho_{\mathrm{nf}}\left(u\frac{\partial v}{\partial x}+v\frac{\partial v}{\partial y}\right)&=-\frac{\partial p}{\partial y}+\mu_{\mathrm{nf}}\left(\frac{\partial^2 v}{\partial x^2}+\frac{\partial^2 v}{\partial y^2}\right)\\&+\left[-(\rho_{\mathrm{p},0}-\rho_{\mathrm{f},0})(C-C_0)+(1-C_0)\rho_{\mathrm{f},0}\beta(T_{\mathrm{nf}}-T_{\mathrm{c}})\right]g\end{aligned} \tag{3}$$

$$\begin{aligned}u\frac{\partial T_{\mathrm{nf}}}{\partial x}+v\frac{\partial T_{\mathrm{nf}}}{\partial y}&=\frac{k_{\mathrm{nf}}}{(\rho c)_{\mathrm{nf}}}\left(\frac{\partial^2 T_{\mathrm{nf}}}{\partial x^2}+\frac{\partial^2 T_{\mathrm{nf}}}{\partial y^2}\right)\\&+\tau\left\{D_{\mathrm{B}}\left(\frac{\partial C}{\partial x}\frac{\partial T_{\mathrm{nf}}}{\partial x}+\frac{\partial C}{\partial y}\frac{\partial T_{\mathrm{nf}}}{\partial y}\right)\right.\\&\left.+\frac{D_{\mathrm{T}}}{T_{\mathrm{c}}}\left[\left(\frac{\partial T_{\mathrm{nf}}}{\partial x}\right)^2+\left(\frac{\partial T_{\mathrm{nf}}}{\partial y}\right)^2\right]\right\}\end{aligned} \tag{4}$$

$$u\frac{\partial C}{\partial x}+v\frac{\partial C}{\partial y}=D_{\mathrm{B}}\left(\frac{\partial^2 C}{\partial x^2}+\frac{\partial^2 C}{\partial y^2}\right)+\frac{D_{\mathrm{T}}}{T_{\mathrm{c}}}\left(\frac{\partial^2 T_{\mathrm{nf}}}{\partial x^2}+\frac{\partial^2 T_{\mathrm{nf}}}{\partial y^2}\right) \tag{5}$$

where the nomenclature section provides variables' definitions. The governing equations of the flow of nanofluid and heat transfer inside the porous medium layer are developed as follows:

$$\frac{\partial u}{\partial x}+\frac{\partial v}{\partial y}=0 \tag{6}$$

$$\frac{\rho_{\mathrm{nf}}}{\varepsilon^2}\left(u\frac{\partial u}{\partial x}+v\frac{\partial u}{\partial y}\right)=-\frac{\partial p}{\partial x}+\frac{\mu_{\mathrm{nf}}}{\varepsilon}\left(\frac{\partial^2 u}{\partial x^2}+\frac{\partial^2 u}{\partial y^2}\right)-\frac{\mu_{\mathrm{nf}}}{K}u \tag{7}$$

$$\begin{aligned}\frac{\rho_{\mathrm{nf}}}{\varepsilon^2}\left(u\frac{\partial v}{\partial x}+v\frac{\partial v}{\partial y}\right)&=-\frac{\partial p}{\partial y}+\frac{\mu_{\mathrm{nf}}}{\varepsilon}\left(\frac{\partial^2 v}{\partial x^2}+\frac{\partial^2 v}{\partial y^2}\right)-\frac{\mu_{\mathrm{nf}}}{K}v\\&+\left[-(\rho_{\mathrm{p},0}-\rho_{\mathrm{f},0})(C-C_0)\right.\\&\left.+(1-C_0)\rho_{\mathrm{f},0}\beta(T_{\mathrm{nf}}-T_{\mathrm{c}})\right]g\end{aligned} \tag{8}$$

$$\begin{aligned}&\frac{1}{\varepsilon}\left(u\frac{\partial T_{\mathrm{nf}}}{\partial x}+v\frac{\partial T_{\mathrm{nf}}}{\partial y}\right)\\&=\alpha_{\mathrm{nf}}\left(\frac{\partial^2 T_{\mathrm{nf}}}{\partial x^2}+\frac{\partial^2 T_{\mathrm{nf}}}{\partial y^2}\right)+\tau\left\{D_{\mathrm{B}}\left(\frac{\partial C}{\partial x}\frac{\partial T_{\mathrm{nf}}}{\partial x}+\frac{\partial C}{\partial y}\frac{\partial T_{\mathrm{nf}}}{\partial y}\right)\right.\\&\left.+\left(\frac{D_{\mathrm{T}}}{T_{\mathrm{c}}}\right)\left[\left(\frac{\partial T_{\mathrm{nf}}}{\partial x}\right)^2+\left(\frac{\partial T_{\mathrm{nf}}}{\partial y}\right)^2\right]\right\}+\frac{h_{\mathrm{nfs}}(T_{\mathrm{s}}-T_{\mathrm{nf}})}{\varepsilon(\rho c)_{\mathrm{nf}}}\end{aligned} \tag{9}$$

$$0=\alpha\left(\frac{\partial^2 T_{\mathrm{s}}}{\partial x^2}+\frac{\partial^2 T_{\mathrm{s}}}{\partial y^2}\right)+\frac{h_{\mathrm{nfs}}}{(1-\varepsilon)(\rho c)_{\mathrm{s}}}(T_{\mathrm{nf}}-T_{\mathrm{s}}) \tag{10}$$

$$\begin{aligned}\frac{1}{\varepsilon}\left(u\frac{\partial C}{\partial x}+v\frac{\partial C}{\partial y}\right)&=D_{\mathrm{B}}\left(\frac{\partial^2 C}{\partial x^2}+\frac{\partial^2 C}{\partial y^2}\right)\\&+\left(\frac{D_{\mathrm{T}}}{T_{\mathrm{c}}}\right)\left(\frac{\partial^2 T_{\mathrm{nf}}}{\partial x^2}+\frac{\partial^2 T_{\mathrm{nf}}}{\partial y^2}\right)\end{aligned} \tag{11}$$

Finally, the following equation can be stated for the solid impermeable wall:

$$\frac{\partial^2 T_{\mathrm{w}}}{\partial x^2}+\frac{\partial^2 T_{\mathrm{w}}}{\partial y^2}=0 \tag{12}$$

The corresponding boundary conditions for free nanofluid—porous interface, i.e. $x = s + d$, can be written as follows [63, 64]:

$$\begin{aligned}&u_{\text{free nanofluid}}=u_{\text{porous}},\quad v_{\text{free nanofluid}}=v_{\text{porous}}\\&\mu_{\mathrm{nf}}\left.\frac{\partial u}{\partial n}\right|_{\text{free nanofluid}}=\mu_{\mathrm{nf,eff}}\left.\frac{\partial u}{\partial n}\right|_{\text{porous}},\quad \mu_{\mathrm{nf}}\left.\frac{\partial v}{\partial n}\right|_{\text{free nanofluid}}\\&=\mu_{\mathrm{nf,eff}}\left.\frac{\partial v}{\partial n}\right|_{\text{porous}}\quad T_{\mathrm{nf}}|_{\text{free nanofluid}}=T_{\mathrm{nf}}|_{\text{porous}}=T_{\mathrm{s}}|_{\text{porous}}\\&k_{\mathrm{nf}}\left.\frac{\partial T_{\mathrm{nf}}}{\partial n}\right|_{\text{free nanofluid}}=k_{\mathrm{nf,eff}}\left.\frac{\partial T_{\mathrm{nf}}}{\partial n}\right|_{\text{porous}}+k_{\mathrm{s,eff}}\left.\frac{\partial T_{\mathrm{s}}}{\partial n}\right|_{\text{porous}}=q_i\\&C_{\text{free nanofluid}}=C_{\text{porous}},\quad \left.\frac{\partial C}{\partial n}\right|_{\text{free nanofluid}}=\left.\frac{\partial C}{\partial n}\right|_{\text{porous}}\end{aligned} \tag{13}$$

where $k_{\mathrm{nf,eff}}=\varepsilon k_{\mathrm{nf}}$, $k_{\mathrm{s,eff}}=(1-\varepsilon)k_{\mathrm{s}}$, $\mu_{\mathrm{nf,eff}}=\frac{\mu_{\mathrm{nf}}}{\varepsilon}$.

The third line of the above boundary conditions, Eq. (13), indicates that the temperature of the nanofluid inside the pores, porous matrix and the nanofluid in the clear flow are equal. This assumption can be true due to the fact that the interaction between the fluid and the porous matrix is very high in the interface of the porous medium and clear fluid region. The fourth line indicates that the amount of heat which reaches the clear fluid layer is equal to the amount of heat that carries on through the porous matrix medium layer and the amount of heat that reached the interface due to the fluid inside the pores.

In addition, the boundary conditions associated with the wall-porous interface, i.e. $x = s$, is given by [18, 64]:

$$\begin{aligned}&T_{\mathrm{w}}|_{\text{wall}}=T_{\mathrm{nf}}|_{\text{porous}}=T_{\mathrm{s}}|_{\text{porous}}\\&k_{\mathrm{w}}\left.\frac{\partial T_{\mathrm{w}}}{\partial n}\right|_{\text{wall}}=k_{\mathrm{nf,eff}}\left.\frac{\partial T_{\mathrm{nf}}}{\partial n}\right|_{\text{porous}}+k_{\mathrm{s,eff}}\left.\frac{\partial T_{\mathrm{s}}}{\partial n}\right|_{\text{porous}}=q_i\\&D_{\mathrm{B}}\left.\frac{\partial C}{\partial n}\right|_{\text{porous}}+\frac{D_{\mathrm{T}}}{T_{\mathrm{c}}}\left.\frac{\partial T_{\mathrm{nf}}}{\partial n}\right|_{\text{porous}}=0\end{aligned} \tag{14}$$

The first line of the above boundary conditions, Eq. (14), indicates that the temperature of the nanofluid inside the pores, porous matrix and the solid wall are equal. This

assumption can be true due to the fact that both three layers have merged at the wall interface. Indeed, the fluid velocity at the wall surface is considered as zero, and the porous matrix is also unified with the wall. Hence, assuming a uniform equal temperature for the solid wall, porous matrix and the quiescent nanofluid in the pores next to the wall is a rational assumption. The second line demonstrates the energy balance at the interface surface of the solid wall and porous region. This equation indicates that the amount of heat which reaches the interface through the solid wall is equal to the amount of heat that reaches the porous matrix and the fluid in the pores.

Eventually, the boundary conditions applied to the external walls of the cavity are.

$$\begin{cases} T_{\mathrm{w}}(0,y) = T_{\mathrm{h}} & z - b/2 \le y \le z + b/2 \\ \dfrac{\partial T_{\mathrm{w}}(0,y)}{\partial x} = 0 & y \ge z + b/2 \text{ and } y \le z - b/2 \end{cases}$$

$$u(L,y) = v(L,y) = 0, \quad T_{\mathrm{nf}}(L,y) = T_{\mathrm{c}},$$

$$D_{\mathrm{B}}\frac{\partial C(L,y)}{\partial x} + \frac{D_{\mathrm{T}}}{T_{\mathrm{c}}}\frac{\partial T_{\mathrm{nf}}(L,y)}{\partial x} = 0$$

$$u(X,0) = v(X,0) = 0, \quad \frac{\partial T_{\mathrm{w}}(x,0)}{\partial y} = \frac{\partial T_{\mathrm{nf}}(x,0)}{\partial y} = \frac{\partial T_{\mathrm{s}}(x,0)}{\partial y} = 0, \quad \frac{\partial C(x,0)}{\partial y} = 0 \tag{15}$$

$$u(x,L) = v(x,L) = 0, \quad \frac{\partial T_{\mathrm{w}}(x,L)}{\partial y} = \frac{\partial T_{\mathrm{nf}}(x,L)}{\partial y} = \frac{\partial T_{\mathrm{s}}(x,L)}{\partial y} = 0, \quad \frac{\partial C(x,L)}{\partial y} = 0$$

According to [41, 65], the boundary condition of $D_{\mathrm{B}}\frac{\partial C(L,y)}{\partial x} + \frac{D_{\mathrm{T}}}{T_{\mathrm{c}}}\frac{\partial T_{\mathrm{nf}}(L,y)}{\partial x}$ represents the zero flux of nanoparticles on the wall surfaces. A homogeneous uniform concentration of nanoparticles (C_0) is assumed in the cavity. As the walls are impermeable to the base fluid and nanoparticles, the following constraint should be hold true in all times, with the steady state solution: $\frac{1}{L^2}\int_0^1\int_0^1 C\,\mathrm{d}x\mathrm{d}y = C_0$. In order to non-dimensionalize the governing Eqs. (1)–(12) and the corresponding boundary conditions (13)–(15), the following dimensionless parameters are utilized:

$$X = \frac{x}{L}, \quad Y = \frac{y}{L}, \quad D = \frac{d}{L}, \quad S = \frac{s}{L}, \quad B = \frac{b}{L},$$
$$Z = \frac{z}{L}, \quad U = \frac{uL}{\alpha_{nf}}, \quad V = \frac{vL}{\alpha_{\mathrm{nf}}},$$
$$P = \frac{pL^2}{\rho_{\mathrm{nf}}\alpha_{\mathrm{nf}}^2}, \quad Pr = \frac{\nu_{\mathrm{nf}}}{\alpha_{\mathrm{nf}}}, \; Da = \frac{K}{L^2}, \; \phi = \frac{C}{C_0},$$
$$Ra = \frac{(1-C_0)\rho_{\mathrm{f},0} g\beta\Delta T L^3}{\alpha_{\mathrm{nf}}\mu_{\mathrm{nf}}},$$
$$\theta_{\mathrm{nf}} = (T_{\mathrm{nf}} - T_{\mathrm{c}})/\Delta T, \quad \theta_{\mathrm{s}} = (T_{\mathrm{s}} - T_{\mathrm{c}})/\Delta T,$$
$$\theta_{\mathrm{w}} = (T_{\mathrm{w}} - T_{\mathrm{c}})/\Delta T,$$
$$Nr = \frac{(\rho_{\mathrm{p},0} - \rho_{\mathrm{f},0})C_0}{\rho_{\mathrm{f},0}\beta\Delta T(1-C_0)}, \quad Nb = \frac{\tau D_{\mathrm{B}} C_0}{\alpha_{\mathrm{nf}}}, Nt = \frac{\tau D_{\mathrm{T}}\Delta T}{\alpha_{\mathrm{nf}}\, T_{\mathrm{c}}},$$
$$H = \frac{h_{\mathrm{nfs}}L^2}{k_{\mathrm{nf}}}, \quad K_{\mathrm{r}} = \frac{k_{\mathrm{nf}}}{(1-\varepsilon)k_{\mathrm{s}}}, \quad Le = \frac{\alpha_{\mathrm{nf}}}{D_{\mathrm{B}}}, R_{\mathrm{k}} = \frac{k_{\mathrm{w}}}{k_{\mathrm{nf}}} \tag{16}$$

where $\Delta T = T_{\mathrm{h}} - T_{\mathrm{c}}$. Based on the non-dimensional variables of Eq. (16), the dimensionless forms of Eqs. (1)–(12) are obtained as follows:

Nanofluid domain:

$$\frac{\partial U}{\partial X} + \frac{\partial V}{\partial Y} = 0 \tag{17}$$

$$U\frac{\partial U}{\partial X} + V\frac{\partial U}{\partial Y} = -\frac{\partial P}{\partial X} + Pr\left(\frac{\partial^2 U}{\partial X^2} + \frac{\partial^2 U}{\partial Y^2}\right) \tag{18}$$

$$U\frac{\partial V}{\partial X} + V\frac{\partial V}{\partial Y} = -\frac{\partial P}{\partial Y} + Pr\left(\frac{\partial^2 V}{\partial X^2} + \frac{\partial^2 V}{\partial Y^2}\right) - Ra\cdot Pr\cdot Nr(\phi - 1) + Ra\cdot Pr\cdot\theta_{\mathrm{nf}} \tag{19}$$

$$U\frac{\partial \theta_{\mathrm{nf}}}{\partial X} + V\frac{\partial \theta_{\mathrm{nf}}}{\partial Y} = \frac{\partial^2\theta_{\mathrm{nf}}}{\partial X^2} + \frac{\partial^2\theta_{\mathrm{nf}}}{\partial Y^2} + Nb\left(\frac{\partial\phi}{\partial X}\frac{\partial\theta_{\mathrm{nf}}}{\partial X} + \frac{\partial\phi}{\partial Y}\frac{\partial\theta_{\mathrm{nf}}}{\partial Y}\right) + Nt\left[\left(\frac{\partial\theta_{\mathrm{nf}}}{\partial X}\right)^2 + \left(\frac{\partial\theta_{\mathrm{nf}}}{\partial Y}\right)^2\right] \tag{20}$$

$$U\frac{\partial\phi}{\partial X} + V\frac{\partial\phi}{\partial Y} = \frac{1}{Le}\left(\frac{\partial^2\phi}{\partial X^2} + \frac{\partial^2\phi}{\partial Y^2}\right) + \frac{Nt}{Le\cdot Nb}\left(\frac{\partial^2\theta_{\mathrm{nf}}}{\partial X^2} + \frac{\partial^2\theta_{\mathrm{nf}}}{\partial Y^2}\right) \tag{21}$$

Porous medium layer:

$$\frac{\partial U}{\partial X} + \frac{\partial V}{\partial Y} = 0 \tag{22}$$

$$\frac{1}{\varepsilon^2}\left(U\frac{\partial U}{\partial X} + V\frac{\partial U}{\partial Y}\right) = -\frac{\partial P}{\partial X} + \frac{Pr}{\varepsilon}\left(\frac{\partial^2 U}{\partial X^2} + \frac{\partial^2 U}{\partial Y^2}\right) - \frac{Pr}{Da}U \tag{23}$$

$$\frac{1}{\varepsilon^2}\left(U\frac{\partial V}{\partial X}+V\frac{\partial V}{\partial Y}\right)=-\frac{\partial P}{\partial Y}+\frac{Pr}{\varepsilon}\left(\frac{\partial^2 V}{\partial X^2}+\frac{\partial^2 V}{\partial Y^2}\right)-\frac{Pr}{Da}V - Ra\cdot Pr\cdot Nr(\phi-1)+Ra\cdot Pr\cdot\theta_{\mathrm{nf}} \tag{24}$$

$$U\frac{\partial\theta_{\mathrm{nf}}}{\partial X}+V\frac{\partial\theta_{\mathrm{nf}}}{\partial Y} =\varepsilon\left(\frac{\partial^2\theta_{\mathrm{nf}}}{\partial X^2}+\frac{\partial^2\theta_{\mathrm{nf}}}{\partial Y^2}\right)+Nb\cdot\varepsilon\left(\frac{\partial\phi}{\partial X}\frac{\partial\theta_{\mathrm{nf}}}{\partial X}+\frac{\partial\phi}{\partial Y}\frac{\partial\theta_{\mathrm{nf}}}{\partial Y}\right) + Nt\cdot\varepsilon\left[\left(\frac{\partial\theta_{\mathrm{nf}}}{\partial X}\right)^2+\left(\frac{\partial\theta_{\mathrm{nf}}}{\partial Y}\right)^2\right]+H(\theta_{\mathrm{s}}-\theta_{\mathrm{nf}}) \tag{25}$$

$$0=\frac{\partial^2\theta_{\mathrm{s}}}{\partial X^2}+\frac{\partial^2\theta_{\mathrm{s}}}{\partial Y^2}+H\cdot K_{\mathrm{r}}(\theta_{\mathrm{nf}}-\theta_{\mathrm{s}}) \tag{26}$$

$$U\frac{\partial\phi}{\partial X}+V\frac{\partial\phi}{\partial Y}=\frac{\varepsilon}{Le}\left(\frac{\partial^2\phi}{\partial X^2}+\frac{\partial^2\phi}{\partial Y^2}\right) + \frac{Nt\cdot\varepsilon}{Le\cdot Nb}\left(\frac{\partial^2\theta_{nf}}{\partial X^2}+\frac{\partial^2\theta_{nf}}{\partial Y^2}\right) \tag{27}$$

Solid wall layer:

$$\frac{\partial^2\theta_{\mathrm{w}}}{\partial X^2}+\frac{\partial^2\theta_{\mathrm{w}}}{\partial Y^2}=0 \tag{28}$$

In addition, the boundary conditions in dimensionless state are obtained as follows:

Free nanofluid-porous interface boundary conditions:

$$\begin{aligned}
&U_{\text{free nanofluid}}=U_{\text{porous}},\quad V_{\text{free nanofluid}}=V_{\text{porous}}\\
&\left.\frac{\partial U}{\partial N}\right|_{\text{free nanofluid}}=\frac{1}{\varepsilon}\left.\frac{\partial U}{\partial N}\right|_{\text{porous}},\quad \left.\frac{\partial V}{\partial N}\right|_{\text{free nanofluid}}=\frac{1}{\varepsilon}\left.\frac{\partial V}{\partial N}\right|_{\text{porous}}\\
&\theta_{\mathrm{nf}}|_{\text{free nanofluid}}=\theta_{\mathrm{nf}}|_{\text{porous}}=\theta_s|_{\text{porous}}\\
&\left.\frac{\partial\theta_{\mathrm{nf}}}{\partial N}\right|_{\text{free nanofluid}}=\varepsilon\left.\frac{\partial\theta_{\mathrm{nf}}}{\partial N}\right|_{\text{porous}}+K_{\mathrm{r}}^{-1}\left.\frac{\partial\theta_{\mathrm{s}}}{\partial N}\right|_{\text{porous}}=Q_{\mathrm{i}}\\
&\phi_{\text{free nanofluid}}=\phi_{\text{porous}},\quad \left.\frac{\partial\phi}{\partial N}\right|_{\text{free nanofluid}}=\left.\frac{\partial\phi}{\partial N}\right|_{\text{porous}}
\end{aligned} \tag{29}$$

where $Q_{\mathrm{i}}=q_{\mathrm{i}}L/k_{\mathrm{nf}}\Delta T$.

The wall-porous interface boundary condition is:

$$\begin{aligned}
&\theta_{\mathrm{w}}|_{\text{wall}}=\theta_{\mathrm{nf}}|_{\text{porous}}=\theta_{\mathrm{s}}|_{\text{porous}}\\
&R_{\mathrm{k}}\left.\frac{\partial\theta_{\mathrm{w}}}{\partial N}\right|_{\text{wall}}=\varepsilon\left.\frac{\partial\theta_{\mathrm{nf}}}{\partial N}\right|_{\text{porous}}+K_{\mathrm{r}}^{-1}\left.\frac{\partial\theta_{\mathrm{s}}}{\partial N}\right|_{\text{porous}}=\frac{q_{\mathrm{i}}L}{k_{\mathrm{nf}}\Delta T}=Q_{\mathrm{i}}\\
&Nb\left.\frac{\partial\phi}{\partial N}\right|_{\text{porous}}+Nt\left.\frac{\partial\theta_{\mathrm{nf}}}{\partial N}\right|_{\text{porous}}=0
\end{aligned} \tag{30}$$

Other boundary conditions on the vertical and horizontal walls include:

$$\begin{aligned}
&\begin{cases}\theta_{\mathrm{w}}(0,Y)=1 & Z-B/2\le Y\le Z+B/2\\ \dfrac{\partial\theta_{\mathrm{w}}(0,Y)}{\partial X}=0 & Y\ge Z+B/2 \text{ or } Y\le Z-B/2\end{cases}\\
&U(1,Y)=V(1,Y)=0,\quad \theta_{\mathrm{nf}}(1,Y)=0,\\
&Nb\frac{\partial\phi(1,Y)}{\partial X}+Nt\frac{\partial\theta_{\mathrm{nf}}(1,Y)}{\partial X}=0\\
&U(X,0)=V(X,0)=0,\quad \frac{\partial\theta_{\mathrm{w}}(X,0)}{\partial Y}=\frac{\partial\theta_{\mathrm{nf}}(X,0)}{\partial Y}\\
&=\frac{\partial\theta_{\mathrm{s}}(X,0)}{\partial Y}=0,\quad \frac{\partial\phi(X,0)}{\partial Y}=0\\
&U(X,1)=V(X,1)=0,\quad \frac{\partial\theta_{\mathrm{w}}(X,1)}{\partial Y}=\frac{\partial\theta_{\mathrm{nf}}(X,1)}{\partial Y}\\
&=\frac{\partial\theta_{\mathrm{s}}(X,1)}{\partial Y}=0,\quad \frac{\partial\phi(X,1)}{\partial Y}=0
\end{aligned} \tag{31}$$

The non-dimensional constraints of $\int_0^1\int_0^1\phi\mathrm{d}X\mathrm{d}Y=1$ for the overall volume fraction of nanoparticles should also hold true in the steady state solution. In this report, the physical quantities of interest are the heat transfer through the wall, Nusselt number of the nanofluid and solid phases in the interface boundary of the wall as well as the porous medium, and finally Nusselt number of the free nanofluid, which are, respectively, listed below:

$$\begin{aligned}
&Q_{\mathrm{w}}=\frac{q''L}{k_{\mathrm{w}}\Delta T}=\frac{-k_{\mathrm{w}}\left(\frac{\partial T_{\mathrm{w}}}{\partial x}\right)_{\mathrm{x=0,d}}L}{k_{\mathrm{w}}\Delta T}=\left(-\frac{\partial\theta_{\mathrm{w}}}{\partial X}\right)_{\mathrm{X=0,D}}\\
&Nu_{\mathrm{nf}}|_{\text{porous}}=\frac{hL}{k_{\mathrm{nf}}}=\frac{q''L}{k_{\mathrm{nf}}\Delta T}=\frac{-k_{\mathrm{nf}}\left(\frac{\partial T_{\mathrm{nf}}}{\partial x}\right)_{\mathrm{x=d,d+s}}L}{k_{\mathrm{nf}}\Delta T}\\
&=\left(-\frac{\partial\theta_{\mathrm{nf}}}{\partial X}\right)_{\mathrm{X=D,D+S}}\\
&Nu_{\mathrm{s}}=\frac{q''L}{k_{\mathrm{s}}\Delta T}=\frac{-k_{\mathrm{s}}\left(\frac{\partial T_{\mathrm{s}}}{\partial x}\right)_{\mathrm{x=d,d+s}}L}{k_{\mathrm{s}}\Delta T}=\left(-\frac{\partial\theta_{\mathrm{s}}}{\partial X}\right)_{\mathrm{X=D,D+S}}\\
&Nu_{\mathrm{nf}}|_{\text{free nanofluid}}=\frac{hL}{k_{\mathrm{nf}}}=\frac{q''L}{k_{\mathrm{nf}}\Delta T}=\frac{-k_{\mathrm{nf}}\left(\frac{\partial T_{\mathrm{nf}}}{\partial x}\right)_{\mathrm{x=d+s,L}}L}{k_{\mathrm{nf}}\Delta T}\\
&=\left(-\frac{\partial\theta_{\mathrm{nf}}}{\partial X}\right)_{\mathrm{X=D+S,1}}
\end{aligned} \tag{32}$$

$$\overline{Q_{\mathrm{w}}}=\int_0^1 Q_{\mathrm{w}}\,\mathrm{d}y,\ \overline{Nu}=\int_0^1 Nu\,\mathrm{d}y \tag{33}$$

Eventually, using Eqs. (29) and (30):

$$\overline{Q_{\mathrm{w}}}=\varepsilon R_{\mathrm{k}}^{-1}\overline{Nu_{\mathrm{nf}}}|_{\text{porous}}+R_{\mathrm{k}}^{-1}K_{\mathrm{r}}^{-1}\overline{Nu_{\mathrm{s}}}\ \text{at}\ X=D \tag{34}$$

$$\overline{Nu_{\mathrm{nf}}}|_{\text{free nanofluid}}=\varepsilon\overline{Nu_{\mathrm{nf}}}|_{\text{porous}}+K_{\mathrm{r}}^{-1}\overline{Nu_{\mathrm{s}}}\ \text{at}\ X=D+S \tag{35}$$

It is notable that the values of Sherwood number are not included in this investigation since according to the boundary conditions given in Eqs. (30) and (31), $Sh = \frac{Nt}{Nb} Nu$. In addition, considering the steady state solution and based on the energy conservation, it can be deduced that $\left|\left(-\frac{\partial\theta_w}{\partial X}\right)_{X=0}\right| = \left|\left(-\frac{\partial\theta_w}{\partial X}\right)_{X=D}\right|$ and $\left|\left(-\frac{\partial\theta_{nf}}{\partial X}\right)_{X=D+S}\right| = \left|\left(-\frac{\partial\theta_{nf}}{\partial X}\right)_{X=1}\right|$. Thus, the results would only be reported for the Nusselt numbers at the interface of the free fluid and the porous layer at $X = D + S$. The other values of important heat transfer characteristics can be evaluated using the above relations.

Numerical approach, grid independence test and validation

The governing equations, Eqs. (17) and (18), are nonlinear and coupled to each other; hence, it is essential to apply a numerical approach to solve them, which are associated with the boundary conditions expressed as (29)–(31). Here, the Galerkin finite element method was utilized to solve the equations with the corresponding boundary conditions. This method has been explained in details in [66–68]. The quadrilateral structural elements were employed to discretize the computational domain such that the compression of the elements near the solid walls and internal interface was more than that of other regions. However, before starting calculations in order to obtain the results, the grid independence test was conducted to evaluate the solution sensitivity to the grid and ensure the accuracy of the results. The grid check was performed for the following set of non-dimensional parameters: $Z = 0.5$, $B = \varepsilon = 0.6$, $Ra = 10^6$, $Da = 10^{-2}$, $Nr = Nb = Nt = K_r = 0.1$, $Le = H = R_k = 10$ and $Pr = 6.2$. As displayed in Table 1, the test was performed for five grids with different grid elements numbers. Evaluation of the variations of three quantities of $\overline{Nu_{nf}}|_{\text{free nanofluid}}$, $\overline{Nu_{nf}}|_{\text{porous}}$ and $|\psi|_{max}$ showed that error was less than 0.3% when the grid size was 90 × 90. Hence, according to the solution accuracy and the time required for convergence, the grid size 90 × 90 has been utilized to perform the calculations.

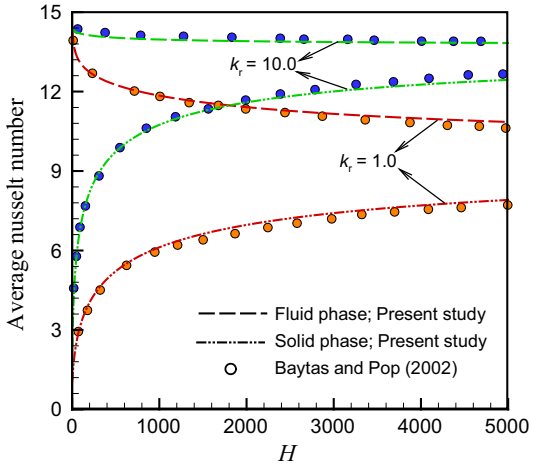

Fig. 2 Measurement of the obtained values of average Nusselt number versus H from the present study with the study conducted by Baytas and Pop [12]

The results of the present numerical solution were compared with the findings presented in the literature [12, 13, 18]. Considering a regular fluid ($Nt = 0$) and setting $D = 0$, $S = B = 1$ and $Z = 0.5$ (the entire of the hot wall was at the hot temperature $\theta_w = 1$, and the cavity was filled with a porous medium layer), the present study reduces to the study of Baytas and Pop [12]. Hence, the first validation consists of the comparison between average Nusselt number versus H for the results reported by Baytas and Pop [12] and those obtained here. The results of this comparison are illustrated in Fig. 2 when $Ra \times Da = 10^3$ and $Da = 10^{-4}$.

Considering a triangular cavity saturated with a porous medium filled with a nanofluid (without a free fluid or solid layer), the results of our research can be compared with the results of Sheremet and Pop [13]. Hence, in another validation, Fig. 3 evaluates the results obtained for local Nusselt number with the data reported by Sheremet and Pop [13] when $Nr = Nb = Nt = 0.1$ and $Le = 1.0$.

Considering the conjugate heat transfer of a regular fluid in a cavity, the results of the present study can be compared with the results of Saeid [18]. In the study of Saeid, the bottom and top walls of the cavity were insulated, while the right and left walls were isothermal with temperature difference. Each of the cold and hot walls was covered with a

Table 1 Grid independency test when $Z = 0.5$, $B = \varepsilon = 0.6$, $Ra = 10^6$, $Da = 10^{-2}$, $Nr = Nb = Nt = K_r = 0.1$, $Le = H = R_k = 10$ and $Pr = 6.2$

Grid	$\overline{Nu_{nf}}\|_{\text{free nanofluid}}$	Error/%	$\overline{Nu_{nf}}\|_{\text{porous}}$	Error/%	$\|\psi\|_{max}$	Error/%
30 × 30	9.8489		5.2138		25.553	
50 × 50	9.7345	1.162	5.1124	1.945	24.590	3.769
70 × 70	9.6347	1.025	5.0557	1.109	24.268	1.309
90 × 90	9.6418	0.0737	5.0545	0.024	24.206	0.255
110 × 110	9.6475	0.0591	5.0550	9.89E−03	24.179	0.112

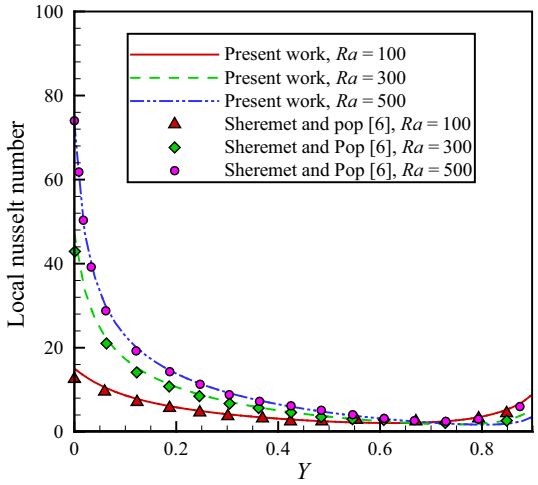

Fig. 3 Comparison of local Nusselt number between the current study and work carried out by Sheremet and Pop [13]

Table 2 Comparison of the results of the present numerical solution and those performed by Saeid [18] at $Ra \times Da = 10^3$, $Da = 10^{-5}$, $D = 0.1$ and $K_r = H = 1$

R_k	$\overline{Nu}_f$	$\overline{Nu}_s$	$\overline{Q}_w$	$\lvert\psi\rvert_{max}$	$\Delta\theta$
Present results					
0.1	0.343	0.113	4.557	3.611	0.03
1	2.903	0.429	3.332	8.006	0.05
10	9.727	1.016	1.074	15.821	0.05
Saeid					
0.1	0.326	0.110	4.357	3.536	0.03
1	2.814	0.418	3.232	7.898	0.05
10	9.887	1.010	1.090	16.219	0.05

solid layer with a thickness S. A layer of porous medium imbued with a regular base fluid was sandwiched between the two solid layers. Neglecting the nanoparticles effects, ($Nt = 0$), and setting $B = 1$, $Z = 0.5$, the present study can be reduced to [18]. By setting $Ra \times Da = 10^3$, $D = 0.1$, $K_r = H = 1$ and $Da = 10^{-5}$, Table 2 revels the values of four parameters $\overline{Nu}_f$, $\overline{Nu}_s$, $\overline{Q}_w$ and $|\psi|_{max}$ for the various values of R_k within the range 0.1–10 in comparison with the results provided by Saeid [18]. In addition, as shown in Fig. 4, the patterns of the isotherms and streamlines concluded from the present modeling have been compared with the work conducted by Saeid [18]. As seen, there is an excellent agreement between the results provided by the present modeling and those represented by the published literature [12, 13, 18].

Results and discussion

Here, the findings of the present numerical investigation have been illustrated in the forms of streamlines, isotherms and isoconcentrations along with the mean Nusselt number of nanofluid at the right wall $\overline{Nu}_{nf}\big|_{\text{free nanofluid}}$, the average Nusselt number of nanofluid in the porous layer $\overline{Nu}_{nf}\big|_{\text{porous}}$ and solid phases of the porous medium $\overline{Nu}_s$ at the solid wall-porous interface boundary. Calculations have been performed for various values of $Ra = 10^3$–10^6; $B = 0.2$–0.8; $Z = 0.3$–0.7; $Le = 10$–100; $K_r = 0.1$–10; $R_k = 0.1$–10, $H = 0.1$–1000, $\varepsilon = 0.3$–0.9 and $Da = 10^{-5}$–10^{-2} and constant values of $Nt = Nb = Nr = 0.1$ and $Pr = 6.2$.

Effects of Rayleigh number

In order to investigate the impact of the buoyancy force on the flow, concentration fields, and temperature, the streamlines, isoconcentrations patterns and isotherms are demonstrated in Fig. 5 for various values of Ra, while the other parameters have been kept constant at $B = 0.4$; $Z = 0.7$; $H = R_k = Le = 10$; $K_r = 1$; $\varepsilon = 0.6$, $Nr = Nb = Nt = 0.1$ and $Da = 10^{-2}$. When Ra is low ($Ra = 10^3$ and 10^4), the conduction mode is predominant, and a weak recirculating flow can be found in the cavity. As shown, an increase in Rayleigh number, representing the buoyancy force, increases the power of the flow circulation. Further, the distance between the streamlines in the porous region is increased. This increase indicates the reduction in the fluid velocity. As the Rayleigh number rises, the existence of the porous layer induces a more significant effect on the streamlines. Within the entire range of the studied Rayleigh numbers, comparatively symmetric patterns of streamlines density next to the vertical walls in the free fluid layer and the porous layer can be observed. However, the distance of the streamlines next to the solid porous interface, i.e. $X = D$, is higher than that of the cold wall at $X = 1$. In other words, the boundary layer in the free flow region is the main difference in the streamlines of the regions of the porous layer and free flow is in the core zones of the cavity, where the buoyancy forces become weak.

It is also clear that with elevation of Rayleigh number, the streamlines next to the vertical walls get closer, indicating that the convection flow is strengthened. At $Ra = 10^6$, the fluid velocity in the middle of the porous region is very low in comparison with the free flow region. This is because of the fact that the pressure drop in a porous medium which is due to the viscous resistance caused via Darcy term grows by the increase in the velocity. As mentioned, in the core region of the cavity, the buoyancy forces are weak and the difference between the streamlines

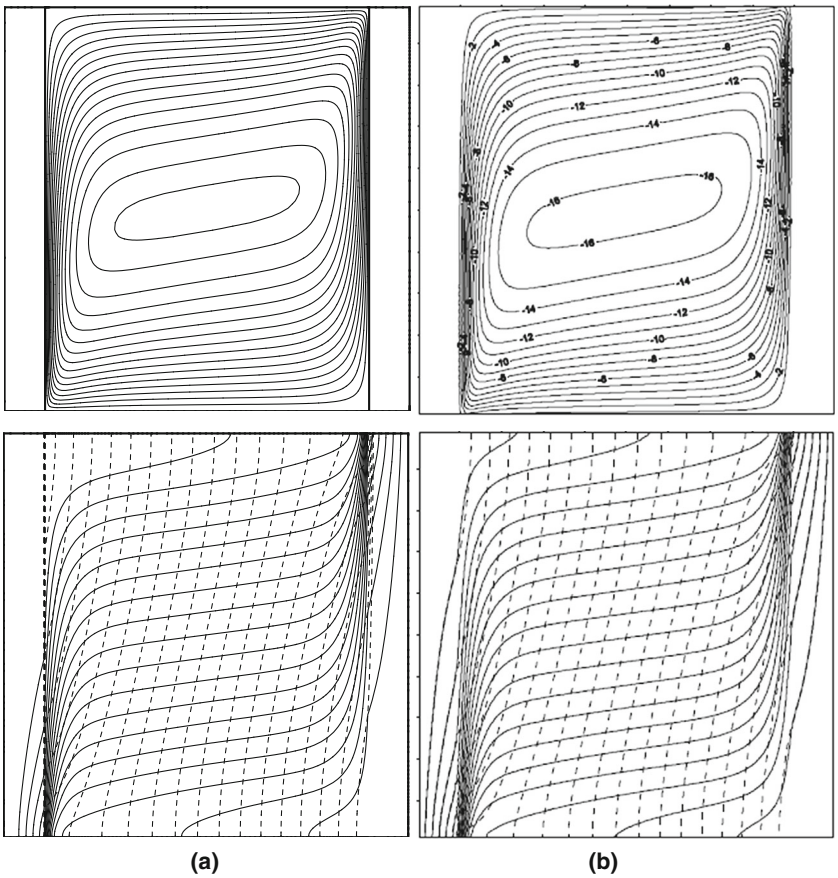

Fig. 4 Comparison of streamlines and isotherms related to **a** the current study and **b** those provided by Saeid [18] at $R_k = 10$, $Ra \times Da = 10^3$, $Da = 10^{-5}$ and $K_r = H = 1$

of the porous layer and the free flow region is more obvious. Another result of increasing the pressure drop in the porous region is the shift of the core of the recirculation cell in the cavity toward the cold wall as shown in Fig. 5. When $Ra = 10^3$, the conduction mode is predominant, the isotherms of the solid phase (dash lines) and the nanofluid are very similar in the porous region, with the difference between those becoming more evident as Ra increases. As Ra grows, lines of isotherms of the nanofluid in the core zone of the cavity tend to possess a stratified pattern. This trend suggests that the dominance of the convection grows by increasing Ra, confirming the formation of horizontal jets at the top and bottom walls of the cavity.

In the temperature contours, the dashed lines reveal the temperature of the solid matrix (θ_s). The continuous lines in the solid region indicate the temperature of the solid wall (θ_w) in the solid layer, while they show the temperature of the nanofluid (θ_{nf}) in the porous layer and the free fluid layer. When Rayleigh number is small, i.e. $Ra = 10^3$, the patterns of the temperature in the solid matrix of the porous medium and the nanofluid are very close. In this case, the conduction mechanism is the dominant mechanism of the heat transfer, while the fluid motion is very smooth. In this studied case, K_r is adopted as unity ($K_r = 1.0$), revealing that the thermal conductivity of the porous matrix is the same as that of the nanofluid. Thus, neglecting the convection effects, the diffusion of the heat absorbed from the hot wall in the solid porous matrix and the nanofluid would be almost the same. In addition, as the fluid motion is low and there is an interactive mechanism between the solid porous matrix and the nanofluid ($H = 10$), the temperatures of the solid porous matrix and the nanofluid are close to each other and follow the same pattern. Nevertheless, as the Rayleigh number rises, the convection mechanism grows stronger and the velocity of the nanofluid also increases. Hence, the weak interface convection heat transfer mechanism (H) between the solid matrix phase and the nanofluid could not significantly affect the temperature patterns of the nanofluid inside the porous layer region, and hence, the temperature patterns of the nanofluid in the porous layer are almost the same as those in the free flow region.

Attention to the contours of the concentration of nanoparticles in the cavity shows that the patterns of this concentration almost follow the pattern of the streamlines. However, there are some deviations due to the Brownian and thermophoresis effects (diffusive terms). It can be seen that the nanoparticles concentration in the vicinity of the hot interface of the solid wall-porous layer is low compared to the cold vertical wall of the cavity. This effect is the

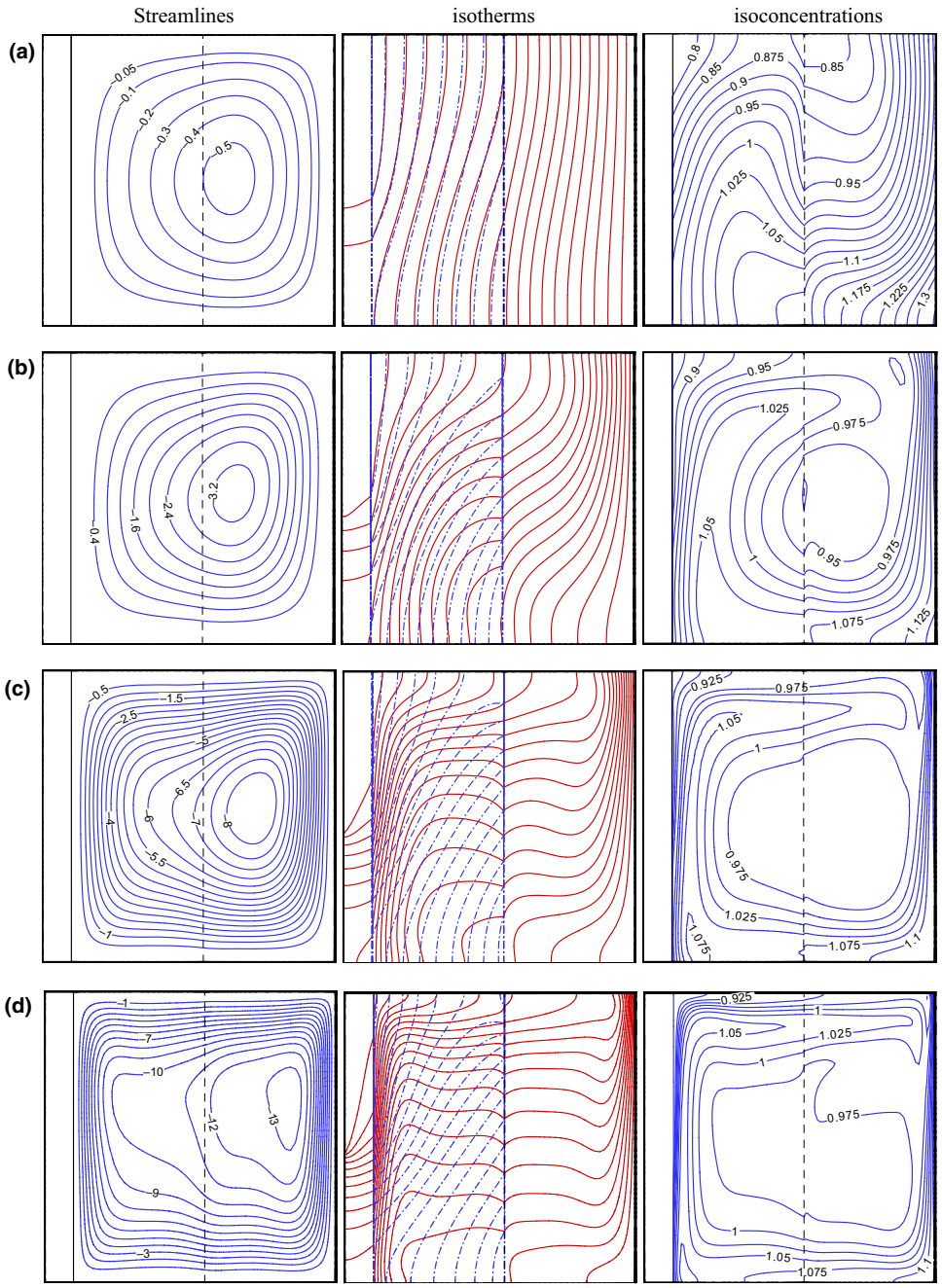

Fig. 5 Display of the streamlines, isotherms and isoconcentrations for **a** $Ra = 10^3$, **b** $Ra = 10^4$, **c** $Ra = 10^5$ and **d** $Ra = 10^6$ at fixed parameters $B = 0.4$; $Z = 0.7$; $R_k = Le = H = 10$; $K_r = 1$, $\varepsilon = 0.6$ and $Da = 10^{-2}$

result of the thermophoresis force. The thermophoresis force typically carries nanoparticles along the direction opposite to the temperature gradient (from hot regions to cold regions). Next to the hot wall, the temperature gradient is toward the hot wall (as the X increases, the temperature decreases), and hence, the nanoparticles tend to move away from the hot wall. Hence, as can be seen, the nanoparticles' concentration is low on the hot wall. In contrast, the concentration of the nanoparticles at the cold wall is high. The core zones of the cavity have nearly a uniform nanoparticles' concentration. In this region, the temperature gradients are smooth, and hence, the Brownian motion has effectively uniformed the nanoparticles in the cavity.

Effects of K_r

To display the effects of K_r on the flow, temperature and nanoparticles' concentration fields, the isotherms, streamlines and isoconcentrations patterns are represented in Fig. 6 when $Ra = 10^6$; $B = 0.5$; $Z = 0.6$; $Le = H{=}R_k = 10$; $\varepsilon = 0.6$ and $Da = 10^{-2}$. As shown, the increase in K_r

decreases the solidity of the recirculation cell, formed inside the cavity. K_r indicates the ratio of the thermal conductivity of the nanofluid to the thermal conductivity of the solid porous matrix. A very low value of K_r represents the great thermal conductivity of the solid porous matrix compared to the nanofluid. This is the case which occurs for metal foams. In this case, the heat conductivity in the phase of the solid porous matrix is very powerful. Hence, the porous medium would channel the heat inside the solid matrix and distribute it in the nanofluid due to the interface convection heat transfer mechanism (H). Thus, the heat transfer can be enhanced and the circulation flows are also strong for the low values of K_r. Further, the temperature contours demonstrate that the temperature patterns of the solid matrix phase (θ_s) are almost parallel to the vertical hot wall when $K_r = 0.1$, which indicates the strong conduction mechanism. The deviation of the temperature curves (from the vertical direction) is due to the interaction between the nanofluid inside the porous medium and the solid porous matrix. As K_r increases, the temperatures in the porous and pure nanofluid region tend to converge. Moreover, a more uniform dispersion of nanoparticles inside the porous layer can be observed when K_r is high. Indeed, for high values of K_r, the temperature gradients inside the nanofluid decrease, and as a result, the thermophoresis force also declines. Thus, in the cavity, one can expect a more uniform nanoparticle distribution.

Effects of the length *B* and the position of the heating element *Z*

The effects of the length and the position of the heating element are discussed in this section for $Ra = 10^5$, $Le = H = K_r = R_k = 10$, $\varepsilon = 0.6$ and $Da = 10^{-2}$. Figure 7 displays the effects of the length of the heating element, while its position has been fixed at $Z = 0.5$. As can be seen, the streamlines, isotherms and isoconcentrations fields have kept their general patterns constant with increasing the length of heating element from 0.2 to 0.8 with the step 0.2. Although the change in the length of the element reveals a smooth effect on the strength and shape of the recirculation cells, the patterns of the isotherms and isoconcentration contours are almost independent of the element length. This is due to the fact that the solid wall acts as a redistributor for the heat absorbed from element and quickly diffuses the absorbed heat inside itself.

Figure 8 depicts the effects of the position of the heating element on the streamlines, isotherms and isoconcentration patterns, while the other parameters have been kept constant at $Ra = 10^5$, $B = 0.5$, $Le = H{=}R_k = 10$, $K_r = 1$, $\varepsilon = 0.6$, $Nt = Nb = Nr = 0.1$, $Da = 10^{-3}$. The shape and strength of the formed circulation cell within the cavity decline by the increase in Z. However, this elevation is not very obvious, and thus the changes in the isotherms and isoconcentration contours are not very significant. It can be observed that the isotherms in the solid layer follow the location of the element. However, the isotherms and isoconcentrations in both of the solid porous matrix and nanofluid phases are almost fixed as the position of the element changes.

Effects of Darcy number

The effects of Darcy number on the streamlines, isotherms and isoconcentration patterns are illustrated in Fig. 9 for the fixed values of $B = 0.5$; $Z = 0.25$; $Nr = Nb = Nt = 0.1$, $H = Le = K_r = R_k = 10$, $\varepsilon = 0.6$, $Ra = 10^6$. According to the figure, the variation of Darcy number, Da, obviously affects the governing patterns of the nanofluid flow. This result arises from extreme variation of the pressure drop caused by the Darcy term in the porous region. Since the density of the streamlines depicts the velocity amplitude of the nanofluid, it can be concluded that when $Da = 10^{-5}$, the solid matrix impedes the fluid motion and diminishes the velocity of the nanofluid substantially in the porous zone. In addition, as the decrease in the pressure drop or hydrodynamic resistance is the result of the rise of the Darcy term, the increase of Da causes augmentation of the size and strength of the recirculation cells formed in the whole of the cavity region. As Darcy number grows, the advection regime becomes stronger within the porous region. The increased difference between thermal fields, i.e. θ_s and θ_{nf}, corresponding to the different values of Da illustrates this fact. It can be seen that the thermal mixing of nanofluid is enhanced in the porous region when Darcy number rises. In addition, it is clear that the distribution of nanoparticles within the cavity entirely depends on the velocity field varying with Darcy number. When $Da = 10^{-5}$, the comparison of isoconcentration lines in the saturated porous and single nanofluid regions clearly demonstrates the effect of the nanofluid velocity on the dispersion of the nanoparticles. As depicted, the nanoparticles' mixing develops by promoting the fluid strength due to the increase in Da.

Figure 10a indicates that the mean Nusselt numbers for both the fluid and solid phases grow as Ra and K_r increase. Indeed, when Ra increases, the strength of the fluid flow is boosted due to the increase in the buoyancy force. Hence, the heat transfer resulting from the convection mode becomes predominant with respect to the conduction mode. Thus, the increase in the average Nusselt number for the nanofluid phase is more than that of the solid porous phase, and the difference between them is intensified as Ra increases. Moreover, as was previously discussed, the increase in K_r enhances the heat transfer and flow circulations in the porous layer, which results in augmentation

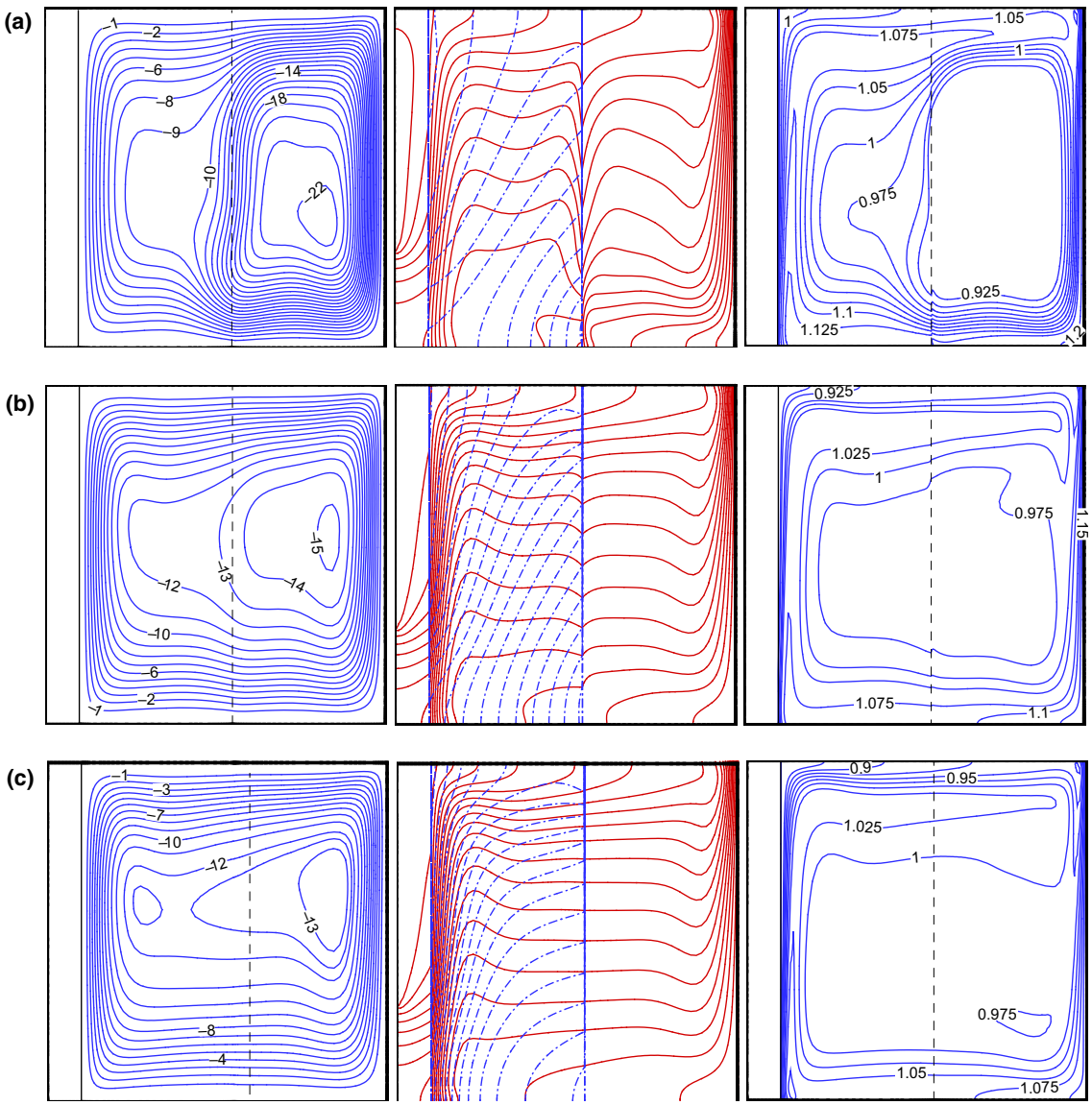

Fig. 6 Display of the streamlines, isotherms and isoconcentrations for two values of **a** $K_r = 0.1$, **b** $K_r = 1$ and **c** $K_r = 10$ at $B = 0.5$; $Z = 0.6$; $Ra = 10^6$, $Le = H/R_k = 10$, $\varepsilon = 0.6$ and $Da = 10^{-2}$

of the mean Nusselt number for two phases of nanofluid and porous medium in the porous region. Since the $\overline{Nu_{nf}}|_{\text{free nanofluid}}$ value is a function of K_r, it is necessary to determine the value of $\overline{Nu_{nf}}|_{\text{free nanofluid}}$ separately. From Fig. 10b, it can be found that the Nusselt number in the right cold boundary has an ascending trend with the increase in K_r. According to Eq. (35), this result is not unexpected. Nonetheless, to justify this trend physically, it should be noted that the increase in K_r indeed represents the increase in the thermal conductivity of the nanofluid compared to that of the solid matrix phase. In the free fluid region, where there is no interface convection heat transfer between the porous matrix and the nanofluid, the growth of the thermal conductivity of the nanofluid would result in overall enhancement of the heat transfer. However, it would reduce the temperature gradient and the average Nusselt number, as the better the thermal diffusion, the more uniform temperature distribution will be. In addition, it is observed that for $K_r > 4$ and for all of the studied Rayleigh numbers, the variations of the average Nusselt number for the fluid phase in the wall-porous interface $\overline{Nu}_{nf}$ and $\overline{Nu_{nf}}|_{\text{free nanofluid}}$ are negligible. However, when Ra is high ($Ra = 10^5$ and 10^6), the average Nusselt Number for the solid phase has a continuously increasing trend with increasing K_r, which is the result of the interface

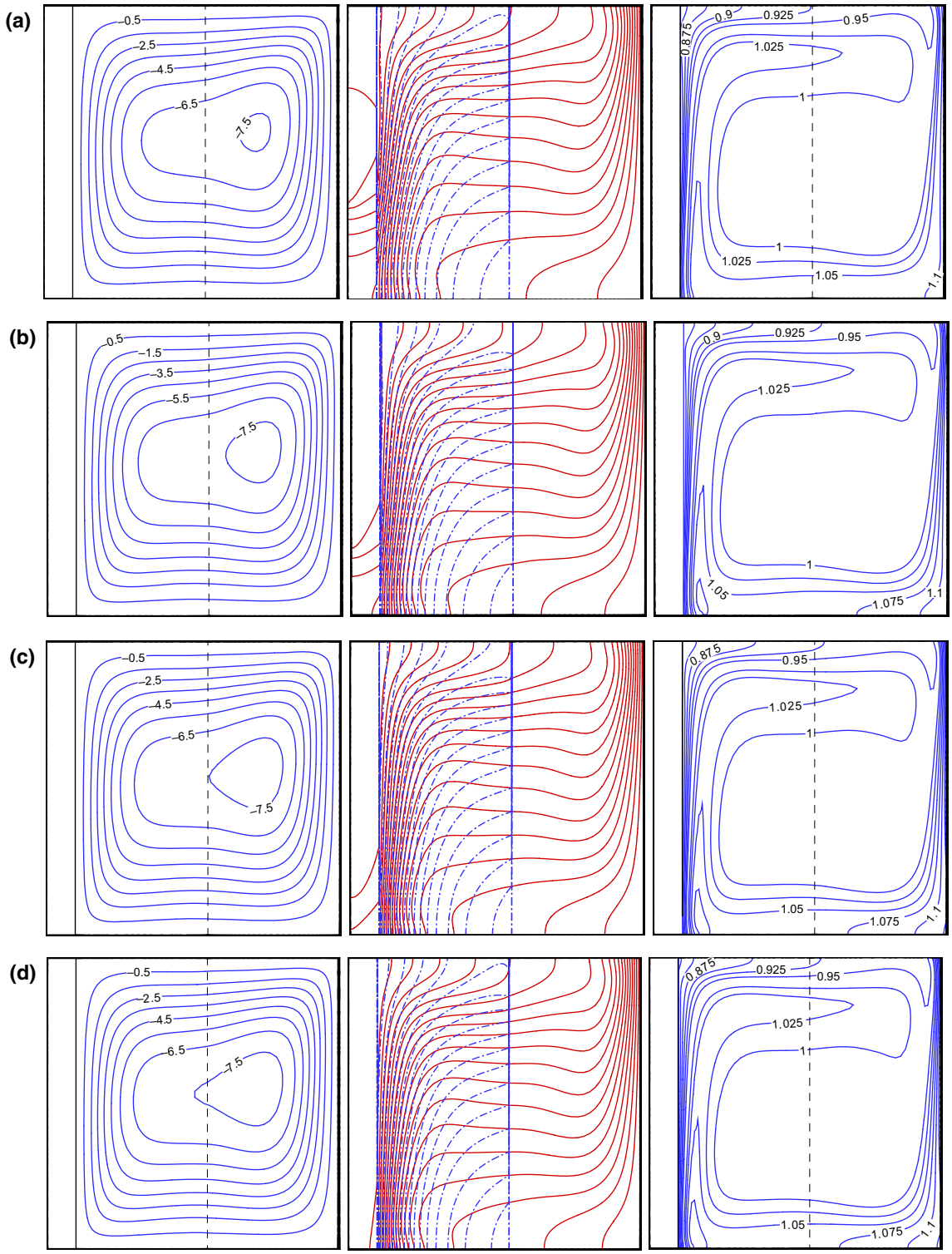

Fig. 7 The effect of the element length (**a** $B = 0.2$, **b** $B = 0.4$, **c** $B = 0.6$ and **d** $B = 0.8$) on the streamlines, isotherms and isoconcentrations at $Ra = 10^5$, $Z = 0.5$, $Le = H{=}K_r = R_k = 10$, $\varepsilon = 0.6$, $Nt = Nb = Nr = 0.1$, $Da = 10^{-2}$

convection heat transfer mechanism between the solid porous matrix and the nanofluid inside the pores ($H = 10$).

The influence of the porosity ε and the length of the heating element B on the mean Nusselt number of nanofluid and the porous medium is demonstrated in Fig. 11,

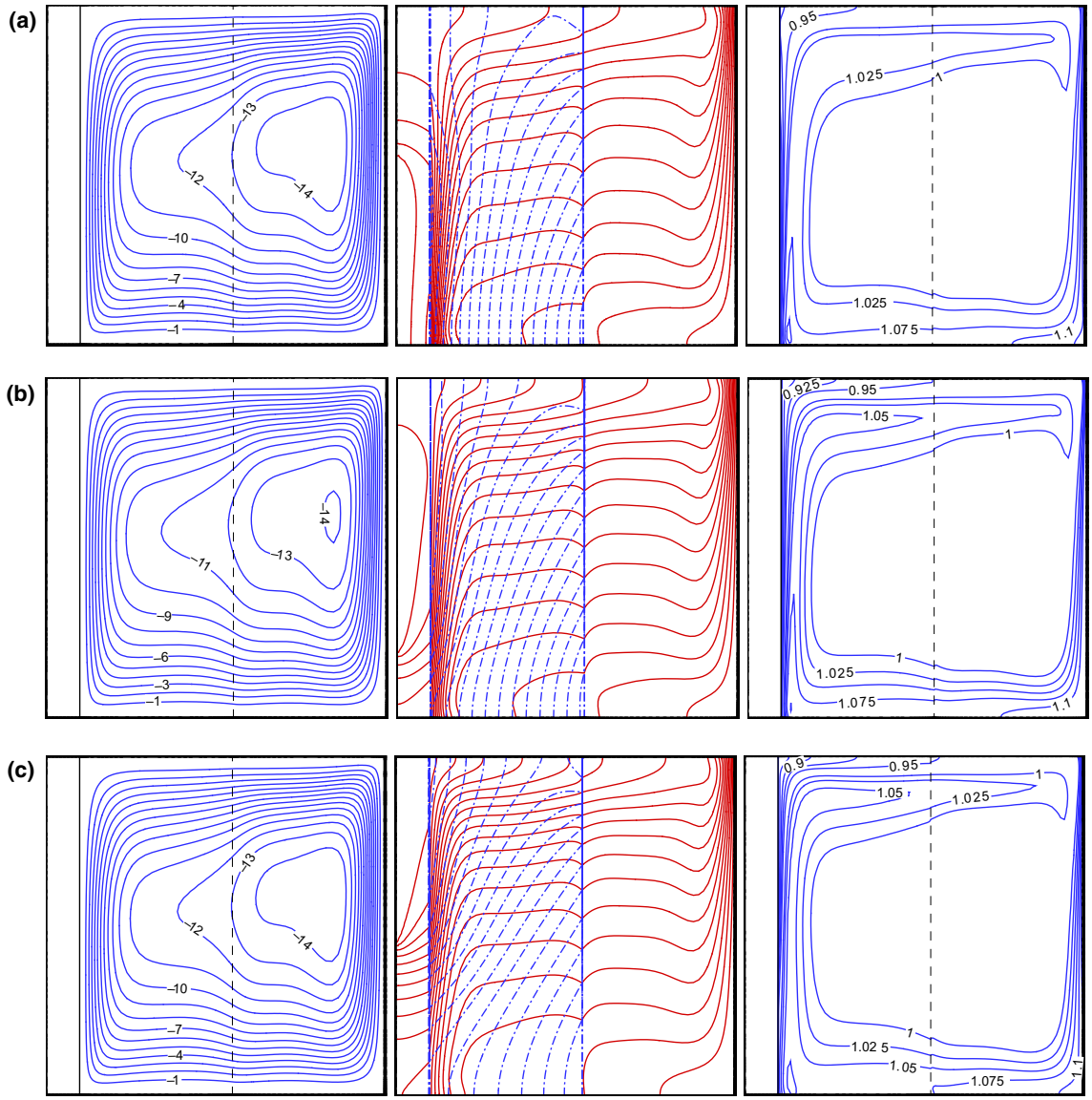

Fig. 8 The effect of the element position (Z) on the streamlines, isotherms and isoconcentrations at **a** $Z = 0.25$, **b** $Z = 0.5$, **c** $Z = 0.75$, $Ra = 10^5$, $B = 0.5$, $Le = H = R_k = 10$, $K_r = 1$, $\varepsilon = 0.6$, $Nt = Nb = Nr = 0.1$, $Da = 10^{-3}$

while the other parameters have been kept constant such that $Ra = 10^5$, $Da = 10^{-2}$, $Nr = Nb = Nt = 0.1$, $K_r = H = Le = R_k = 10$, $Z = 0.5$. This figure demonstrates that the increase in ε can strongly decrease both $\overline{Nu}_{nf}$ and $\overline{Nu}_s$, while the increase in B augments these two Nusselt numbers. The increase in these Nusselt numbers by increasing B is due to the augmentation of the strength of the fluid flow. Indeed, when the strength of the fluid flow rises, the natural convection can transfer more heat.

Figure 12 demonstrates the effect of the position of the heating element and Darcy number on the average Nusselt number of nanofluid and solid phases at the porous region boundary, i.e. $X = S + D$. As seen, the augmentation of Da increases the average Nusselt numbers for both phases. This observed trend is due to the increase in the nanofluid velocity arising from elevation of the permeability of the porous region or reduction in the hydraulic fluid resistance coming from the Darcy term. In addition, it can be observed that the increase in the mean Nusselt number of the nanofluid phase is far larger than that of the porous matrix phase, and the difference between these two Nusselt numbers becomes larger as Da increases. In addition, as shown in Fig. 12, when Da value is low ($Da = 10^{-5}$ and 10^{-4}), the effect of the position of the heating element on the average Nusselt number for the nanofluid phase can be ignored. For all values of Da, the average Nusselt number for the solid phase negligibly varies with the variation in the element heating location. When Da value is high

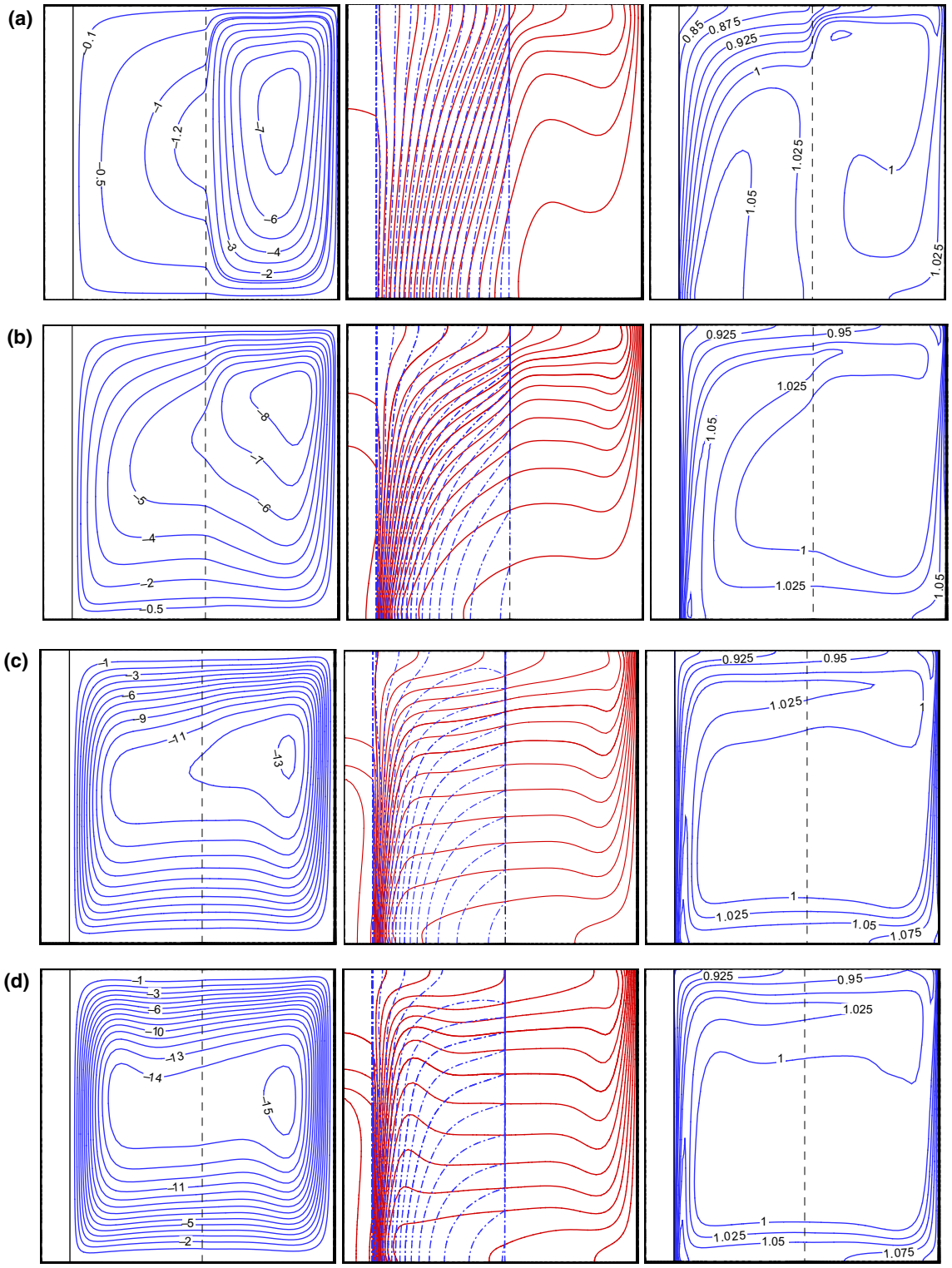

Fig. 9 Display of the streamlines, isotherms and isoconcentrations for various Darcy numbers (**a** $Da = 10^{-5}$, **b** $Da = 10^{-4}$, **c** $Da = 10^{-3}$, **d** $Da = 10^{-2}$) at $B = 0.5$; $Z = 0.25$; $Nr = Nb = Nt = 0.1$, $H = Le = K_r = R_k = 10$, $\varepsilon = 0.6$, $Ra = 10^6$

($Da = 10^{-3}$ and 10^{-2}), the average Nusselt number for the fluid phase increases by the increment in Z from 0.3 to 0.4. Then, the mean Nusselt number stays almost constant when Z reaches 0.5. After this, a decreasing trend can be observed for this number with the growth of Z. In general, it can be deduced that the minimum value of $\overline{Nu}_{nf}$ occurs

when the heating element is located at its maximum position. In addition, it can be said that the maximum value of $\overline{Nu}_{nf}$ occurs at $Z = 0.4$ or 0.5.

Figure 13a, b displays the effect of R_k on the average Nusselt number for the fluid and the solid phases in the interface boundary of wall-porous region for different values of the interphase heat transfer coefficient H. As shown, the average Nusselt numbers rise by increasing R_k. Indeed, the augmentation of R_k means that more heat is transferred to the porous region through the solid wall. In addition, the graphs drawn in Fig. 13a, b depict that the Nusselt number of the fluid phase decreases with increase in H, while the increase in H extremely enhances the Nusselt number of the solid phase. A closer look at the results indicates that the average Nusselt number for the fluid phase remains almost constant with the variations in H when it is in the order of O(0.1) or O(100). In addition, the rise of the mean Nusselt number of the solid phase with the increase of R_k is more evident at the high values of H. According to the definition of $\overline{Q}_w$, an opposite behavior can be observed for the variations of $\overline{Q}_w$ with increasing R_k such that $\overline{Q}_w$ diminish as R_k increases.

The variations in the Nusselt number for the fluid and solid phases at the interface of the wall-porous region as a function of the buoyancy ratio parameter, Nr, are demonstrated in Fig. 14 for the different values of Lewis number Le, while the other parameters have been kept constant. The growth of Nr reduces the mean Nusselt number for both phases. This result can be attributed to the fact that increasing Nr induces a buoyancy force which in some

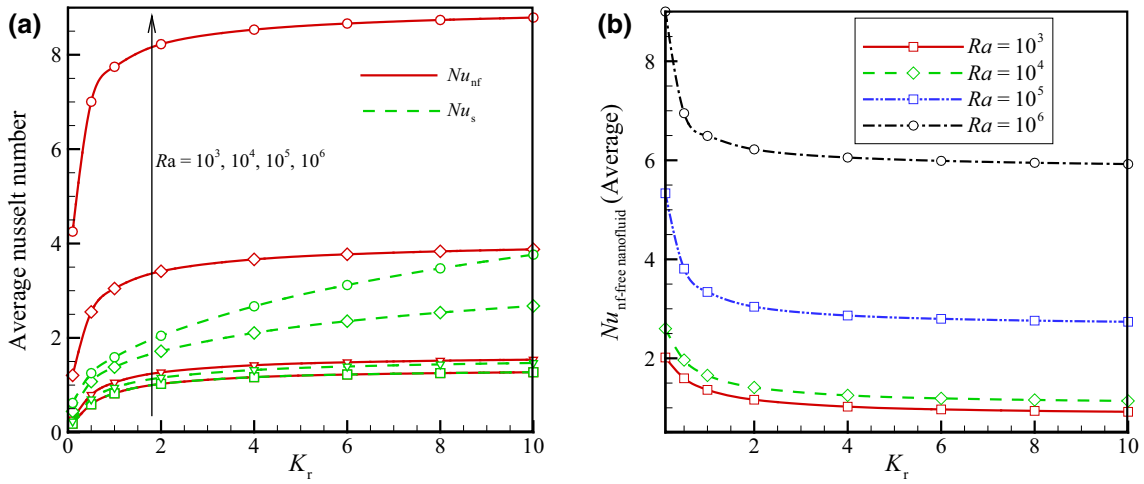

Fig. 10 The variations of **a** $\overline{Nu}_{nf}$ and $\overline{Nu}_s$ and **b** $\overline{Nu}_{nf}|_{\text{free nanofluid}}$ versus K_r for the various values of Ra at $B = Z = 0.5$; $Nr = Nb = Nt = 0.1$, $H = Le = R_k = 10$, $Da = 10^{-3}$, $\varepsilon = 0.6$

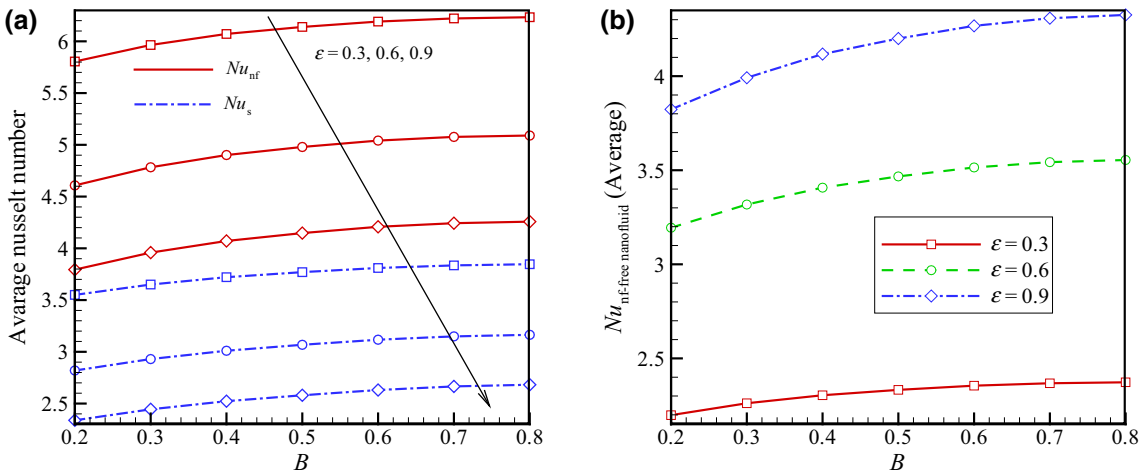

Fig. 11 The variations of **a** $\overline{Nu}_{nf}$ and $\overline{Nu}_s$ and **b** $\overline{Nu}_{nf}|_{\text{free nanofluid}}$ versus B for the various values of ε at $Ra = 10^5$, $Nr = Nb = Nt = 0.1$, $K_r = H = Le = R_k = 10$, $Da = 10^{-2}$, $Z = 0.5$

regions acts against the buoyancy force. Hence, elevation of Nr decreases the strength of the fluid flow, and in response to this reduction, the heat transfer rates declines. In addition, it can be deduced from Fig. 14 that the increment of Lewis number Le enhances the average Nusselt number of both phases. Indeed, the increase in the Lewis number means diminished thickness of the nanoparticles concentration boundary layers over the vertical walls. Consequently, with the reduction in the thickness of the concentration boundary layers, the nanoparticles can transfer the energy more effectively from high- to low-energy regions through their migration. Sheremet et al. [44] have also reported a decreasing trend of the average Nusselt number of nanofluids as a function of Nr for a cavity entirely filled with a LTE porous medium. They have also reported a growing trend for the mean Nusselt number of nanofluids as a function of Lewis number. Accordingly, the patterns of this research findings are in line with the results of [44].

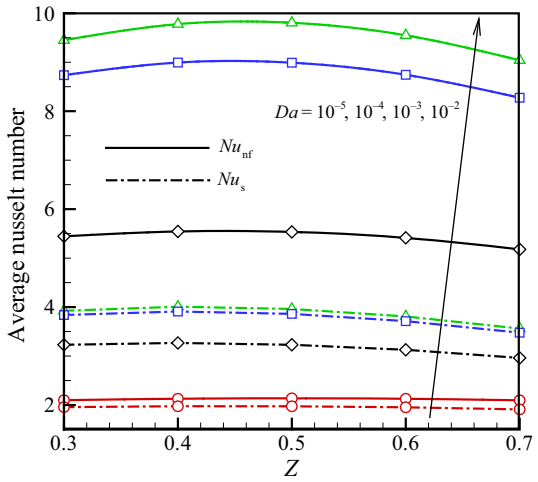

Fig. 12 The variations of $\overline{Nu}_{nf}$ and $\overline{Nu}_{s}$ versus Da for the various values of Z at $Ra = 10^5$, $Nr = Nb = Nt = 0.1$, $K_r = H = Le = R_k = 10$, $B = \varepsilon = 0.6$

Conclusions

In this research, the flow, heat and mass transfer of nanofluids were addressed in a multilayer cavity. The cavity was filled with a layer of solid wall, a layer of porous medium and a layer of free fluid. The layer of the porous medium was saturated by a nanofluid. The local thermal non-equilibrium model was employed for modeling thermal behavior of the porous medium layer. A drift flux of nanoparticles was considered because of the thermophoresis and Brownian motion effects via the Buongiorno's model. The results for the streamlines, the temperature patterns and the concentration of nanoparticles were plotted and discussed. In addition, the Nusselt numbers for the solid porous matrix, the nanofluid inside the porous layer and the nanofluid in the free layer as the important heat transfer properties were also introduced. The impact of the different non-dimensional parameters on the heat transfer properties was discussed further. The main outcomes of this research can be summarized as follows:

1. The non-dimensional nanoparticles' concentration next to the cold wall was about 1.1 which is 10% higher than the average concentration of nanoparticles in the cavity. The non-dimensional concentration of nanoparticles next to the hot wall was low and about 0.92 which is 8% lower than the non-dimensional mean

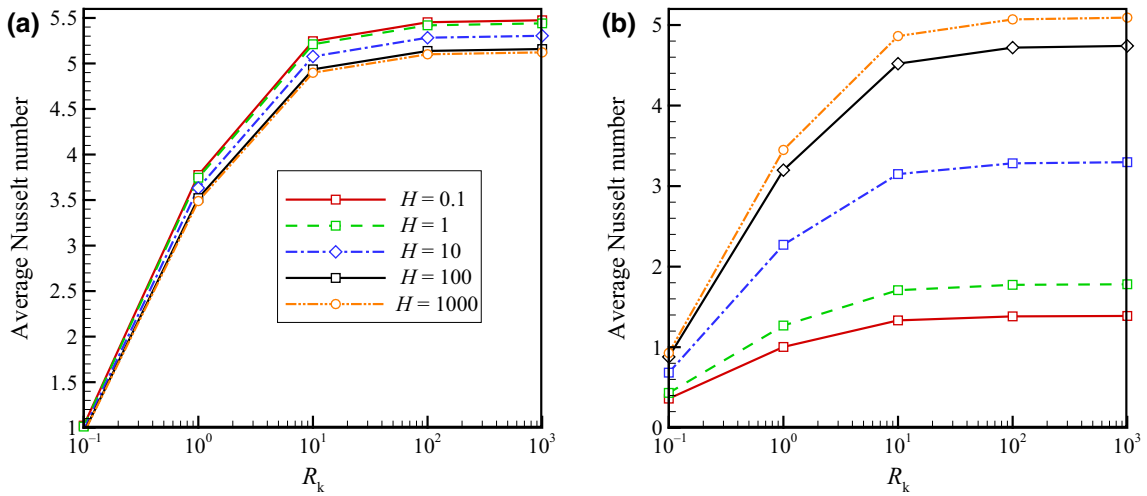

Fig. 13 The variations of $\overline{Nu}_{nf}$ and $\overline{Nu}_{s}$ at $X = D$ versus R_k for the various values of H at $Ra = 10^5$, $Nr = Nb = Nt = 0.1$, $K_r = Le = 10$, $Da = 10^{-2}$, $B = 0.7$, $Z = 0.5$, $\varepsilon = 0.6$

concentration of nanoparticles. When Rayleigh number was small, i.e. $Ra = 10^3$, the concentration gradients were distributed in the cavity. However, as the convection mechanisms became stronger, the distribution of nanoparticles in the core zones of the cavity became uniform, and hence, the concentration gradients were negligible in the core regions of the cavity; however, strong concentration gradients can be seen in the vicinity of the walls.

2. The thermal conductivity ratio of nanofluid/porous matrix, K_r, induced a significant effect on the streamlines and concentration patterns inside the porous layer. The very low values of K_r, i.e. $K_r = 0.1$, resulted in a strong circulation cell in the free fluid layer. In addition, in this case, a considerable concentration gradient of nanoparticles could be observed in the center of the cavity inside the porous layer. The increase in K_r would smoothly reduce the average Nusselt number for the free nanofluid. It should be noticed that the increase in K_r may represent the decrease in the thermal conductivity of the solid porous matrix. In this case, the heat transfer by the solid porous matrix decreased, resulting in the diminished overall heat transfer.
3. Due to the presence of a high thermally conductive solid layer ($R_k = 10$), the length and position of the element did not show obvious effects on the temperature and concentration patterns inside the cavity. The maximum values of the average Nusselt number could be found about $Z = 0.4$ for both phases of the nanofluid and solid matrix. This means that mounting element slightly below the center of the cavity results in greater heat transfer. The increase in the size of the element would also slightly increase the average Nusselt number for the free nanofluid ($Nu_{\text{free nanofluid}}$).
4. Darcy number is very important parameter which plays a significant role in the shape of the streamlines, temperature and concentration patterns. For very low values of Darcy number, i.e. $Da = 10^{-5}$, the velocity in the porous layer significantly decreases. The circulation cells are mainly formed in the free nanofluid layer. The temperature contours in the porous layer would almost show a linear distribution, which confirms the diffusive dominant region of flow. In this case, the concentration gradients of nanoparticles even in the core region of the cavity inside the porous layer could be detected. The increase in Darcy number allowed the fluid to move more freely in the porous layer, and hence, the high values of Darcy number induced a convective heat transfer dominant regime in the porous layer. The increase in Darcy number significantly enhanced the mean Nusselt number for the free nanofluid.
5. The elevation of buoyancy ratio, Nr, resulted in the decrease in mean Nusselt number of the solid porous matrix and the nanofluid inside the porous layer. In contrast, the rise of Lewis number elevated the mean Nusselt number for the both phases at the interface.

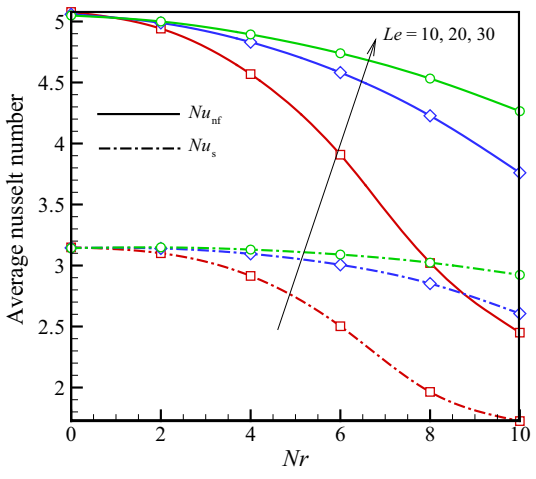

Fig. 14 The variations of $\overline{Nu}_{nf}$ and $\overline{Nu}_s$ at $X = D$ versus Nr for the various values of Le at $Ra = 10^5$, $Nb = Nt = 0.1$, $K_r = H = R_k = 10$, $Da = 10^{-2}$, $B = 0.7$, $Z = 0.5$, $\varepsilon = 0.6$

Acknowledgements Mohammad Ghalambaz is thankful to Dezful Branch Islamic Azad University of the financial support of the present study. The authors are tankful to Iran Nanotechnology Initiative Council (INIC) for its crucial support.

References

1. Mehryan S, et al. Fluid–structure interaction analysis of free convection in an inclined square cavity partitioned by a flexible impermeable membrane with sinusoidal temperature heating. Meccanica. 2017;52(11–12):2685–703.
2. Mehryan S, et al. Analysis of fluid–solid interaction in MHD natural convection in a square cavity equally partitioned by a vertical flexible membrane. J Magn Magn Mater. 2017;424:161–73.
3. Chamkha A, et al. Phase-change heat transfer of single/hybrid nanoparticles-enhanced phase-change materials over a heated horizontal cylinder confined in a square cavity. Adv Powder Technol. 2017;28(2):385–97.
4. Ghalambaz M, et al. Phase-change heat transfer in a cavity heated from below: the effect of utilizing single or hybrid nanoparticles as additives. J Taiwan Inst Chem Eng. 2017;72:104–15.
5. Babcsán N, Beke S, Makk P. Method of producing a metal foam by oscillations and thus obtained metal foam product. Google Patents; 2015.
6. Babcsan N, et al. Pilot production and properties of ALUHAB aluminium foams. Procedia Mater Sci. 2014;4:127–32.
7. Sheikholeslami M, Shehzad S. Simulation of water based nanofluid convective flow inside a porous enclosure via non-equilibrium model. Int J Heat Mass Transf. 2018;120:1200–12.

8. Sheikholeslami M, Seyednezhad M. Simulation of nanofluid flow and natural convection in a porous media under the influence of electric field using CVFEM. Int J Heat Mass Transf. 2018;120:772–81.
9. Sheikholeslami M. Numerical investigation for CuO-H_2O nanofluid flow in a porous channel with magnetic field using mesoscopic method. J Mol Liq. 2018;249:739–46.
10. Nield DA, Bejan A. Convection in porous media. New York: Springer; 2006.
11. Sheremet MA, Trifonova TA. Unsteady conjugate natural convection in a vertical cylinder partially filled with a porous medium. Numer Heat Transf A Appl. 2013;64(12):994–1015.
12. Baytas AC, Pop I. Free convection in a square porous cavity using a thermal nonequilibrium model. Int J Therm Sci. 2002;41(9):861–70.
13. Sheremet MA, Pop I. Free convection in a triangular cavity filled with a porous medium saturated by a nanofluid: Buongiorno's mathematical model. Int J Numer Methods Heat Fluid Flow. 2015;25(5):1138–61.
14. Mehryan S, Izadi M, Sheremet MA. Analysis of conjugate natural convection within a porous square enclosure occupied with micropolar nanofluid using local thermal non-equilibrium model. J Mol Liq. 2018;250:353–68.
15. Hashemi H, Namazian Z, Mehryan S. Cu-water micropolar nanofluid natural convection within a porous enclosure with heat generation. J Mol Liq. 2017;236:48–60.
16. Mehryan S, et al. Free convection of hybrid Al_2O_3–Cu water nanofluid in a differentially heated porous cavity. Adv Powder Technol. 2017;28(9):2295–305.
17. Vafai K. Handbook of porous media. Boca Raton: CRC Press; 2015.
18. Saeid NH. Conjugate natural convection in a porous enclosure sandwiched by finite walls under thermal nonequilibrium conditions. J Porous Media. 2008;11(3):259–75
19. Yang K, Vafai K. Analysis of heat flux bifurcation inside porous media incorporating inertial and dispersion effects—an exact solution. Int J Heat Mass Transf. 2011;54(25):5286–97.
20. Nield D. A note on local thermal non-equilibrium in porous media near boundaries and interfaces. Transport in porous media; 2012: p. 1–4.
21. Lomascolo M, et al. Review of heat transfer in nanofluids: conductive, convective and radiative experimental results. Renew Sustain Energy Rev. 2015;43:1182–98.
22. Angayarkanni S, Philip J. Review on thermal properties of nanofluids: recent developments. Adv Coll Interface Sci. 2015;225:146–76.
23. Öztop HF, et al. A brief review of natural convection in enclosures under localized heating with and without nanofluids. Int Commun Heat Mass Transf. 2015;60:37–44.
24. Sheikholeslami M, Darzi M, Sadoughi M. Heat transfer improvement and pressure drop during condensation of refrigerant-based nanofluid; an experimental procedure. Int J Heat Mass Transf. 2018;122:643–50.
25. Sheikholeslami M, Rokni HB. CVFEM for effect of Lorentz forces on nanofluid flow in a porous complex shaped enclosure by means of non-equilibrium model. J Mol Liq. 2018;254:446–62.
26. Sheikholeslami M, Rokni HB. Numerical simulation for impact of Coulomb force on nanofluid heat transfer in a porous enclosure in presence of thermal radiation. Int J Heat Mass Transf. 2018;118:823–31.
27. Sheikholeslami M, Shehzad S. Numerical analysis of Fe_3O_4–H_2O nanofluid flow in permeable media under the effect of external magnetic source. Int J Heat Mass Transf. 2018;118:182–92.
28. Sheikholeslami M, Rokni HB. Magnetic nanofluid flow and convective heat transfer in a porous cavity considering Brownian motion effects. Phys Fluids. 2018;30(1):012003.
29. Saidur R, Leong K, Mohammad H. A review on applications and challenges of nanofluids. Renew Sustain Energy Rev. 2011;15(3):1646–68.
30. Sheremet MA, Pop I, Shenoy A. Natural convection in a wavy open porous cavity filled with a nanofluid: Tiwari and Das' nanofluid model. Eur Phys J Plus. 2016;131:62.
31. Izadi M, et al. Numerical study of developed laminar mixed convection of Al_2O_3/water nanofluid in an annulus. Chem Eng Commun. 2013;200(7):878–94.
32. Izadi M, Behzadmehr A, Shahmardan M. Effects of inclination angle on laminar mixed convection of a nanofluid flowing through an annulus. Chem Eng Commun. 2015;202(12):1693–702.
33. Izadi M, Behzadmehr A, Shahmardan MM. Effects of discrete source-sink arrangements on mixed convection in a square cavity filled by nanofluid. Korean J Chem Eng. 2014;31(1):12–9.
34. Buongiorno J. Convective transport in nanofluids. J Heat Transfer. 2006;128(3):240–50.
35. Izadi M, et al. Nanoparticle migration and natural convection heat transfer of Cu-water nanofluid inside a porous undulant-wall enclosure using LTNE and two-phase model. J Mol Liq. 2018;261:357–72.
36. Hoghoughi G, et al. Effect of geometrical parameters on natural convection in a porous undulant-wall enclosure saturated by a nanofluid using Buongiorno's model. J Mol Liq. 2018;255:148–59.
37. Noghrehabadi A, Izadpanahi E, Ghalambaz M. Analyze of fluid flow and heat transfer of nanofluids over a stretching sheet near the extrusion slit. Comput Fluids. 2014;100:227–36.
38. Sheremet MA, Pop I, Shenoy A. Unsteady free convection in a porous open wavy cavity filled with a nanofluid using Buongiorno's mathematical model. Int Commun Heat Mass Transf. 2015;67:66–72.
39. Sheremet MA, Pop I, Rahman M. Three-dimensional natural convection in a porous enclosure filled with a nanofluid using Buongiorno's mathematical model. Int J Heat Mass Transf. 2015;82:396–405.
40. Pop I, Ghalambaz M, Sheremet M. Free convection in a square porous cavity filled with a nanofluid using thermal non equilibrium and Buongiorno models. Int J Numer Methods Heat Fluid Flow. 2016;26(3/4):671–93.
41. Sabour M, Ghalambaz M. Natural convection in a triangular cavity filled with a nanofluid-saturated porous medium using three heat equation model. Can J Phys. 2016;94(6):604–15.
42. Sheremet M, Cimpean D, Pop I. Free convection in a partially heated wavy porous cavity filled with a nanofluid under the effects of Brownian diffusion and thermophoresis. Appl Therm Eng. 2017;113:413–8.
43. Zaraki A, et al. Theoretical analysis of natural convection boundary layer heat and mass transfer of nanofluids: effects of size, shape and type of nanoparticles, type of base fluid and working temperature. Adv Powder Technol. 2015;26(3):935–46.
44. Sheremet MA, Groşan T, Pop I. Free convection in shallow and slender porous cavities filled by a nanofluid using Buongiorno's model. J Heat Transf. 2014;136(8):082501.
45. Alsabery A, et al. Heatline visualization of conjugate natural convection in a square cavity filled with nanofluid with sinusoidal temperature variations on both horizontal walls. Int J Heat Mass Transf. 2016;100:835–50.
46. Alsabery A, et al. Transient natural convective heat transfer in a trapezoidal cavity filled with non-Newtonian nanofluid with sinusoidal boundary conditions on both sidewalls. Powder Technol. 2017;308:214–34.
47. Sheikholeslami M, Ganji D. Numerical approach for magnetic nanofluid flow in a porous cavity using CuO nanoparticles. Mater Des. 2017;120:382–93.

48. Sheikholeslami M, Chamkha AJ. Flow and convective heat transfer of a ferro-nanofluid in a double-sided lid-driven cavity with a wavy wall in the presence of a variable magnetic field. Numer Heat Transf A Appl. 2016;69(10):1186–200.
49. Bondareva NS, et al. Heatline visualization of natural convection in a thick walled open cavity filled with a nanofluid. Int J Heat Mass Transf. 2017;109:175–86.
50. Sheikholeslami M, Chamkha AJ. Influence of Lorentz forces on nanofluid forced convection considering Marangoni convection. J Mol Liq. 2017;225:750–7.
51. Reddy PS, Chamkha AJ. Heat and mass transfer characteristics of nanofluid over horizontal circular cylinder. Ain Shams Eng J. 2016;5:505–13.
52. Reddy PS, Chamkha AJ, Al-Mudhaf A. MHD heat and mass transfer flow of a nanofluid over an inclined vertical porous plate with radiation and heat generation/absorption. Adv Powder Technol. 2017;28(3):1008–17.
53. Sheremet MA, Pop I, Roşca NC. Magnetic field effect on the unsteady natural convection in a wavy-walled cavity filled with a nanofluid: Buongiorno's mathematical model. J Taiwan Insti Chem Eng. 2016;61:211–22.
54. Sheremet MA, Revnic C, Pop I. Free convection in a porous wavy cavity filled with a nanofluid using Buongiorno's mathematical model with thermal dispersion effect. Appl Math Comput. 2017;299:1–15.
55. Kasaeian A, et al. Nanofluid flow and heat transfer in porous media: a review of the latest developments. Int J Heat Mass Transf. 2017;107:778–91.
56. Sheikholeslami M. CuO-water nanofluid flow due to magnetic field inside a porous media considering Brownian motion. J Mol Liq. 2018;249:921–9.
57. Sheikholeslami M. Numerical investigation of nanofluid free convection under the influence of electric field in a porous enclosure. J Mol Liq. 2018;249:1212–21.
58. Chamkha AJ, Selimefendigil F, Ismael MA. Mixed convection in a partially layered porous cavity with an inner rotating cylinder. Numer Heat Transf A Appl. 2016;69(6):659–75.
59. Chamkha AJ, Ismael MA. Natural convection in differentially heated partially porous layered cavities filled with a nanofluid. Numer Heat Transf A Appl. 2014;65(11):1089–113.
60. Alsabery A, et al. Heatline visualization of natural convection in a trapezoidal cavity partly filled with nanofluid porous layer and partly with non-Newtonian fluid layer. Adv Powder Technol. 2015;26(4):1230–44.
61. Ismael MA, Chamkha AJ. Conjugate natural convection in a differentially heated composite enclosure filled with a nanofluid. J Porous Media. 2015;18(7):699–716.
62. Sheikholeslami M, Shamlooei M, Moradi R. Fe_3O_4-ethylene glycol nanofluid forced convection inside a porous enclosure in existence of Coulomb force. J Mol Liq. 2018;249:429–37.
63. Alazmi B, Vafai K. Analysis of fluid flow and heat transfer interfacial conditions between a porous medium and a fluid layer. Int J Heat Mass Transf. 2001;44(9):1735–49.
64. Betchen L, Straatman AG, Thompson BE. A nonequilibrium finite-volume model for conjugate fluid/porous/solid domains. Numer Heat Transf A Appl. 2006;49(6):543–65.
65. Kuznetsov A, Nield D. The Cheng–Minkowycz problem for natural convective boundary layer flow in a porous medium saturated by a nanofluid: a revised model. Int J Heat Mass Transf. 2013;65:682–5.
66. Reddy JN. An introduction to the finite element method, vol. 2. New York: McGraw-Hill; 1993.
67. Rao SS. The finite element method in engineering. Amsterdam: Elsevier; 2010.
68. Wriggers P. Nonlinear finite element methods. New York: Springer; 2008.